Structural health modeling of the Ölfusá Suspension Bridge

Damage detection and monitoring aspects

Kristján Uni Óskarsson

Faculty of Civil and Environmental Engineering
University of Iceland
2012

Structural health modeling of the Ölfusá Suspension Bridge

Kristján Uni Óskarsson

30 ECTS thesis submitted in partial fulfillment of a
Magister Scientiarum degree in Structural Engineering

Advisors
Bjarni Bessason
Baldvin Einarsson

Faculty Representative
Einar Þór Ingólfsson

Faculty of Civil and Environmental Engineering
School of Engineering and Natural Sciences
University of Iceland
Reykjavik, May 2012

Structural health modeling of the Ölfusá Suspension Bridge - Damage detection and monitoring aspects
Structural health modeling of the Ölfusá Suspension Bridge
30 ECTS thesis submitted in partial fulfillment of a *Magister Scientiarum* degree in structural engineering

Faculty of Civil and Environmental Engineering
School of Engineering and Natural Sciences
University of Iceland
VR-II, Hjarðarhaga 2-6
107, Reykjavik
Iceland

Telephone: +354 525 4000

Bibliographic information:
Óskarsson, K.U., 2012, Structural health modeling of the Ölfusá Suspension Bridge – Damage detection and monitoring aspects,
Master's thesis, Faculty of Civil and Environmental Engineering, University of Iceland, 79 pages.

Printing: Háskólaprent ehf.
Reykjavik, Iceland, May 2012

Abstract

This thesis serves as one part in an ongoing research project conducted to evaluate the structural health of the Ölfusá Suspension Bridge, where a combination of deterioration and the installation of a heavier bridge deck in 1992 have caused uncertainties regarding the condition of the main cables. The main focus of the work is firstly to evaluate the structural effects of the weight increase by constructing two finite element models, representing the structural configuration before and after the 1992 renovations. The latter model is also intended to provide a basis for calibration with scheduled vibration tests based on comparison of natural frequencies and modal shapes. This will improve the ability of the model to describe the structural behavior. Secondly, a literature overview of reported structural damage detection- and health monitoring methods is provided, in which the main objective is to summarize available techniques and discuss potential applications. The main results include a 49% increase in self-weight of the main span of the current structure compared to the original, inducing 37% increase in maximum tensile forces lowering the cable factor of safety. Due to the uncertain level of cable deterioration, it is difficult to accurately determine the safety factor so it is concluded that further evaluation of the cable condition is preferable. Constant monitoring is not considered necessary at this time, but more decisive measures will need to be taken if the cable section proves to be severely reduced.

Útdráttur

Verkefnið er liður í áframhaldandi rannsóknum sem ætlað er að meta ástand hengibrúarinnar á Ölfusá þar sem hnignun og aukinn eiginþungi sökum byggingar nýs og þyngra brúargólfs árið 1992 hafa leitt til óvissu um burðargetu kapla. Annars vegar er áhersla lögð á að meta áhrif þyngdaraukningarinnar með uppsetningu tveggja tölvulíkana sem lýsa brúnni fyrir og eftir breytingarnar. Seinna líkanið verður einnig kvarðað við niðurstöður fyrirhugaðra mælinga á eigintíðnum brúarinnar til þess að auka nákvæmni þess við lýsingu á svörun mannvirkisins. Hins vegar er yfirliti yfir þekktar ástandsmats- og vöktunaraðferðir á hengibrúm stillt upp, þeim lýst og fjallað um kosti þeirra og galla með það að markmiði að öðlast yfirsýn og leggja mat á hvaða aðferðir gætu hentað hér á landi. Helstu greiningarniðurstöður benda til 49% aukningar á eiginþunga aðalhafs brúarinnar síðan fyrir uppsetningu nýs brúargólfs sem hefur framkallað 37% aukningu á hámarks kapalkröftum og lækkun brotöryggis kaplanna. Vegna óvissu á burðarþoli kaplanna sökum tæringar og aldurshnignunar er erfitt að leggja nákvæmt mat á brotöryggið og þykir því nauðsynlegt að kanna ástand þeirra nánar. Ekki er talið tímabært sem stendur að ráðast í uppsetningu vöktunarkerfis, en frekari úrræði verða nauðsynleg komi í ljós að veruleg skerðing hafi orðið á þverskurðarflatarmáli og þar af leiðandi burðarþoli kaplanna.

Contents

List of Figures

List of Tables

Acknowledgements

The work presented here is a 30 ECTS thesis submitted in partial fulfillment of a master's degree in structural engineering at the University of Iceland. I would like to thank the people of the Research Fund of the Icelandic Road Administration for supporting the project. I would like to thank Bjarni Bessason at the University of Iceland for his valuable guidance throughout the project, and also Baldvin Einarsson at the University of Iceland and Guðmundur Valur Guðmundsson at the collaborating partner EFLA Consulting Engineers for their assistance. Furthermore I thank my fiancée, Sylvía Dögg and our two children, Elísa Dröfn and Óskar Pálmi for all their support.

1 Introduction

1.1 Background

The Ölfusá Suspension Bridge, built in 1945, serves as an important road connection carrying average daily summer traffic of nearly 11000 vehicles on highway 1 into the town of Selfoss, located around 60 km from Reykjavik. This places the bridge as the oldest, but most heavily loaded suspension bridge on the Icelandic road system. The structural configuration of the bridge includes an 84 m long cable supported main span and three additional I-girder supported side spans. The two lane roadway of the main span was reconstructed in 1992 which involved the installation of a considerably heavier concrete deck. The construction of this newer bridge deck is suspected of having induced significant increase in the tensile forces acting in the main cables and also to have led to uneven force distribution between cable planes because of the unsymmetrical weight distribution of the deck.

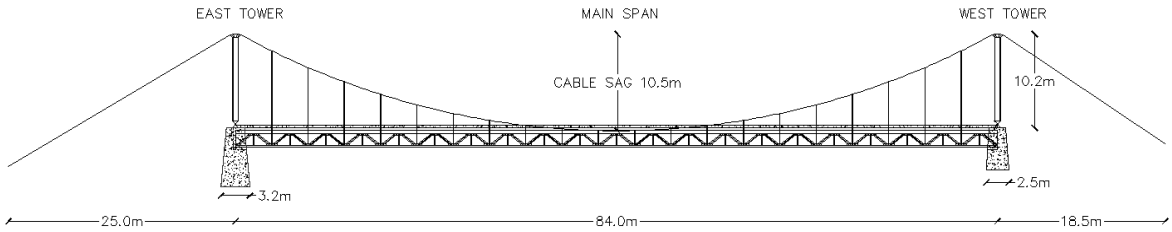

Figure 1-1: Main span of the Ölfusá Suspension Bridge

Uncertainties regarding the structural state of the Ölfusá Bridge have been of some concern, especially regarding the actual condition and bearing capacity of the main cables. The structural condition of the main cables has recently been evaluated subsequent to a visual inspection. A considerable reduction in the cable factor of safety was noted due to increased self-weight and traffic loading. The condition of the cables indicated potential degradation do to corrosion, which could decrease the active cross section of the cables and therefore the bearing capacity. These uncertainties pose concerns regarding the structural integrity of the bridge and suggest that further investigations should be performed.

The preservation of the Ölfusá Bridge may be concluded to be of significant importance for the population in the south of Iceland, being a socially important link with regard to work commuting, tourism and safety precautions. This promotes the necessity of adequate monitoring and maintenance to ensure the structural safety of the bridge while still in service.

1.2 Main objectives

The work presented in this thesis is one part of an ongoing research project which is intended to provide an evaluation on the actual structural condition of the Ölfusá Suspension Bridge. The three main chapters include an introductory discussion on suspension bridges, a structural health oriented finite element model of the bridge, and a literature overview of reported structural damage detection- and health monitoring methods. Main focus will firstly be oriented towards the modeling process and secondly on the literature overview.

The modeling includes two finite element models, one representing the original configuration of the bridge and another one representing the present configuration. The models are assembled using commercial finite element software, utilizing frames, shells, solids, and cables as main elements. Results describing the static and dynamic responses of the structure are obtained by nonlinear analysis of the defined models.

The main purpose of modeling the original configuration of the bridge is to validate the accuracy of the modeling process by comparing with documented test results, and reaction and cable forces from design drawings. Results from the model of the current state of the bridge will then be used to evaluate the severity of increased deformations and cable forces with regard to structural safety of the main cables. Furthermore, the outcome of a modal analysis performed to describe the vibrational characteristics of the current structure will be studied to estimate suitable positioning of accelerometers in scheduled vibration tests. The latter structural model is then intended to provide a reliable basis for calibration with the vibration tests where the simulated model is correlated with corresponding frequency measurements of the structure. This process further improves the ability of the model to accurately describe the actual behavior of the bridge.

The objective of the literature overview of structural damage detection- and health monitoring methods is to systematically summarize available techniques and discuss potential applications. The selection of topics is conducted with regard to the system configuration and structural health of the Ölfusá Suspension Bridge to give a broad perspective on which measures may be appropriate in terms of evaluation and structural life estimation of the bridge.

2 Suspension bridges

In the advancement of bridge engineering, several types of bridges have been developed. Categorization of bridges is carried out according to the structural configuration and mainly differentiates between five types: Beam bridges, cantilever bridges, arch bridges, truss bridges, and cable-supported bridges (Xu & Xia, 2012). Cable supported bridges, divided into cable-stayed bridges and suspension bridges are competitive for long spans (over 200 m) due to the structural configuration and high strength/density ratio of the cables.

The longest suspension bridge in the world is currently the Akashi-Kaikyo Bridge in Kobe, Japan which opened in 1998 and has a main span of 1991 m. The longest cable stayed bridge is the Sutong Bridge in Jiangsu Province, China which opened in 2008 with a main span of 1088 m. Despite these great span lengths already in service, projects involving even longer spans are being considered. One project which has been under evolution for the past decades is a suspension bridge across the Messina Strait between Italy and the island of Sardinia with a free span of 3300 m, giving an indication of future development of long span suspension bridges.

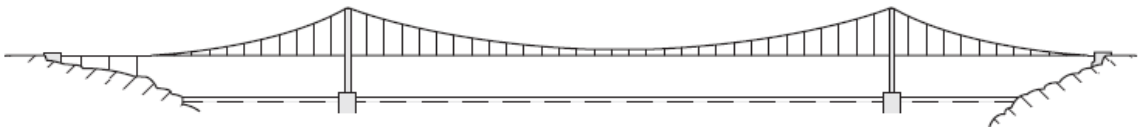

Figure 2-1: Suspension bridge side view (Åkesson, 2008)

2.1 History

Since the construction of the first suspension bridges early in the 1800s, a trend has appeared in ever increasing span lengths, variety in construction materials and adjustment of girder depth to improve aerodynamic stability of the superstructure.

In 1823 the Frenchman Marc Seguin built the first permanent cable supported bridge composed of drawn iron wires in Geneva, Switzerland. In 1826 Thomas Telford designed the Menai Bridge with a main span of 176 m connecting the island of Anglesey and mainland of Wales. Different from the bridge in Geneva, the Menai Bridge used chains assembled from wrought iron eye-bars instead of wires due to lack of corrosion protective measures at that time making the wires less durable than thicker bars. Other notable suspension bridges from the 19th century include the Grand Pont Suspendu across the Sarine Valley in Switzerland completed in 1834 with a main span of 273 m, the Clifton Suspension Bridge across Aron Gorge, Bristol England, opened in 1864 with a span of 214 m and the Wheeling Suspension Bridge across the Ohio River in the USA from 1849 with a span of 308 m. Also the Niagra Bridge, finished in 1855 was a pioneering design by the German bridge designer John A. Roebling. It carried both a roadway and a railroad track over a span of 250 m and was the first major suspension bridge to utilize Roebling´s air spun wire cables. Roebling had a large influence on the advancement of bridge design and

after completing the Cincinnati-Covington Bridge across the Ohio River in 1866 he finished much of the design work of the Brooklyn Bridge before dying in 1869 (Gimsing, 1998).

The Brooklyn Bridge across the East River in New York City was completed in 1883 with three spans of 286 + 486 + 286 m. The design introduced a number of features enhancing the modernization of suspension bridges. From experience of previous projects, Roebling utilized a stiffer cable stayed system in cooperation with the suspension system to improve aerodynamic stability and also his aerial spinning method was used for constructing parallel cables from steel wires. Other bridges over the East River were constructed over the next decades. The Williamsburg Bridge with spans of 284 + 488 + 284 opened in 1903 was the first bridge to use steel towers instead of masonry and in 1909 the Manhattan Bridge opened for traffic. A feature differentiating the Brooklyn Bridge and the Williamsburg Bridge from modern suspension bridges is the arrangement of the main cables at the middle of the span. In these two bridges the cables go all the way down to the bottom chord of the stiffening truss at the middle of the main span reducing the height of the towers opposed to modern bridges where the lowest point of the parabolic cables is kept above the stiffening truss (Gimsing, 1998; Xu & Xia, 2012).

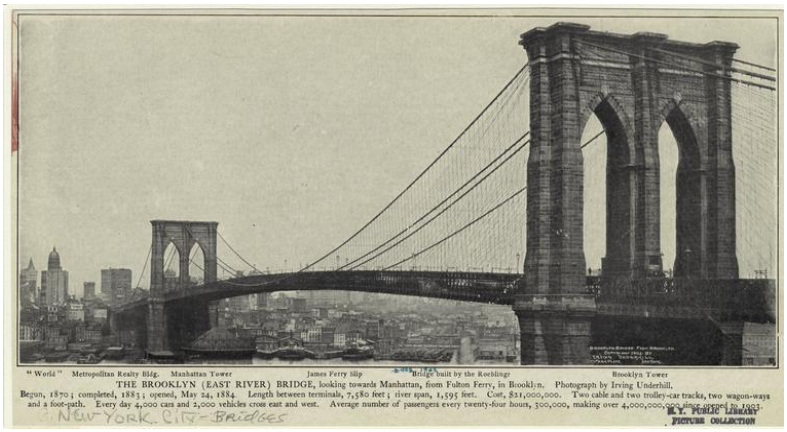

Figure 2-2: Brooklyn Bridge (NYPL Digital Library, 2011)

Up until the design of the Manhattan Bridge, structural analysis of suspension bridges had been based on first order elastic theory. First order theory neglects the change of geometry due to node displacements resulting in very deep stiffening trusses of the long span suspension bridges built in the late 19th century. The deflection theory, developed by Melan in Vienna in 1888 was first put into practice in design of the Manhattan Bridge. Opposed to the first order theories, this second order theory takes account of the deflection of the main cables under traffic load when bending moments of the stiffening girder are calculated. The use of the deflection theory resulted in smaller bending moments in the stiffening girder which led to a huge leap in span lengths in the 1930s when shallower and therefore lighter girders were designed (Gimsing, 1998; Xu & Xia, 2012).

In 1931, the George Washington Suspension bridge was built with a record span length of 1067 meters. Suspension bridge design was now evolving away from the use of robust stiffening girders to shallower girders. Very long bridges were constructed in the next few years such as the San Francisco Oakland Bay Bridge opening in 1936 with two main spans

of 704 m and the Golden Gate Bridge opening in 1937 with a span of 1280 m. With relatively few collapses of suspension bridges since the collapse of the original Wheeling Bridge in 1854 and with the application of the deflection theory in bridge design, a tendency to give less thought to aerodynamic stability had developed among engineers. Designers were tempted to construct more economical suspension bridges with girders of inadequate stiffness which led to the collapse of the 853 m main span of the Tacoma Narrows suspension bridge in 1940. The designer of the bridge relied upon the weight of the long span to ensure stability in wind but the 2,45 m high girders of the bridge were much too flexible causing the bridge deck to oscillate even in small winds. The bridge then collapsed after only four months in service in November 1940 under wind conditions of only 16-19 m/s (Åkesson, 2008).

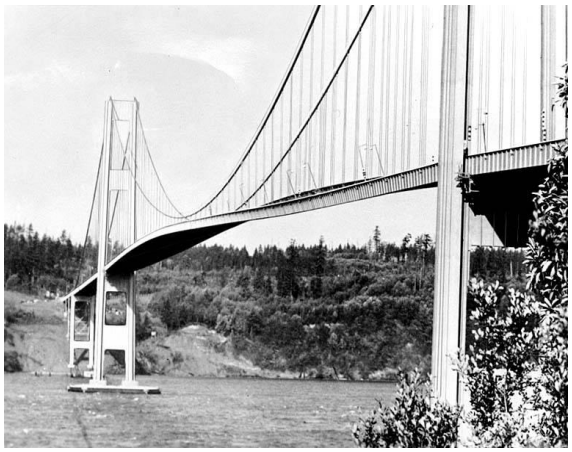

Figure 2-3: Tacoma Narrows Bridge during collapse (Åkesson, 2008)

After the collapse of the Tacoma Narrows Bridge, much more effort was put into aerodynamic studies. Investigations of the stability of recently built bridges were carried out resulting in safety provisions of some bridges including an installation of a lower lateral bracing on the Golden Gate Bridge. After World War II the Tacoma Narrows Suspension bridge was rebuilt and the Mackinac Bridge was constructed with a main span of 1158 m before the Tancarville Bridge in France marked the beginning of further development of large suspension bridges in Europe. The French bridge was built in 1959 with a main span of 608 m and only five years later the Firth of Forth Bridge in Scotland was completed spanning 1006 m. Over the next decades many long span suspension bridges were built in Europe including the Severn Bridge in 1966 where a slender but stiff box girder was introduced instead of a deep stiffening truss. The Humber Bridge was completed in 1981 with the largest free span in the world of 1410 m and more recently the Great Belt Bridge creating a link between Denmark and Sweden was completed in 1998 with a main span of 1624 m. Since the 1970s many long span suspension bridges have been constructed in eastern Asia, especially in China and Japan with the longest current suspension bridge in the world being the Akashi Kaikyo Bridge in Japan spanning almost 2000 m with nearly 300 m high pylons (Gimsing, 1998).

Figure 2-4: Akashi Kaikyo Bridge – the world's longest suspension bridge

2.2 Structural system

According to Gimsing (1998), the structural system of a suspension bridge can be divided into four main components: The Stiffening girder (either consisting of a box girder or a truss), the cable system supporting the stiffening girder, the towers which support the cable system and anchor blocks supporting the cable system. The configuration of the suspension system is characterized by the parabolic main cable running between the anchor blocks on each side of the span and the vertical or slightly inclined suspender cables which connect the stiffening girder to the main cable. Furthermore, the European Steel Design Education Programme (ESDEP) classifies suspension bridges according to the suspension of the girder, anchorage of the main cable and position of expansion joints. A so called S-type configuration has both main and side spans suspended similar to the bridge shown in Figure 2-5 while an F-type configuration only has suspenders over the main span. In modern construction of suspension bridges, earth anchorage is incorporated for transmission of forces to the ground and expansion joints for the stiffening girder can be positioned either at the towers or at the anchor blocks. The Ölfusá Suspension Bridge comprises an earth anchored F-type configuration with girder expansion joints at the towers.

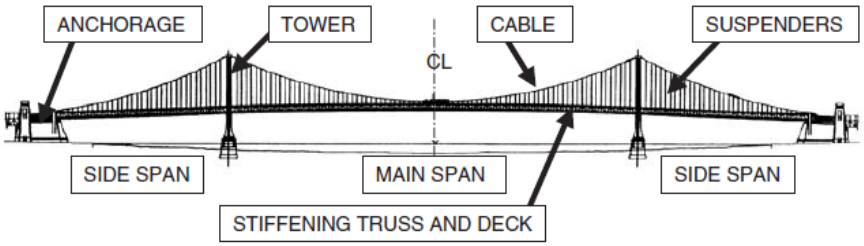

Figure 2-5: Components of a suspension bridge (Mayrbaurl & Camo, 2004)

2.2.1 Stiffening girder and bridge deck

The main function of the stiffening girder is to support the bridge deck carrying traffic loads and provide aerodynamic stability of the superstructure. The girder is subjected to lateral load in the form of wind loading which makes the torsional rigidity an important concern in the design process. Local bending moments due to the traffic loading also affect the design, especially in the case of multiple lane bridges that may comprise very wide decks. In long span suspension bridges it has been common practice to employ either box girders or trusses as stiffening girders. Figure 2-6 shows common cross sections of the stiffening girder/truss. Cross section (a) is built up with two vertical plate girders and a deck plate. This kind of open section is highly susceptible to torsional deformations in longer spans. The box girder section shown in (b) is much stiffer and is used in various formations in longer span suspension bridges. The section in (c) is similar to (a), except that the vertical girders are trusses instead of plate girders providing insignificant torsional stiffness. An extra horizontal truss has been added in (d) to improve the torsional stiffness as was done in the case of some bridges in the 1930s such as the Golden Gate Bridge (Gimsing, 1998 p.305-306). Systems (d) and (b) are the most common in modern suspension bridges and are shortly discussed in the following paragraphs.

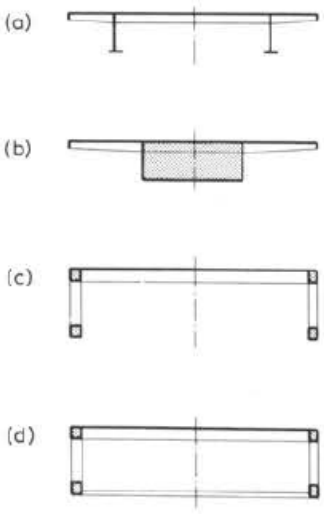

Figure 2-6: Basic cross sections (Gimsing, 1998)

Truss girders and streamlined box girders

In the history of suspension bridge construction, trusses have in long periods been the preferred structural component to ensure flexural and torsional stiffness of the bridge deck. Variations in the depth have characterized the development of truss usage in both suspension and cable stayed bridges as was discussed in chapter 2.1 leading to dangerously shallow trusses in the 1930s. Figure 2-7 shows basic cross sections for stiffening trusses commonly used in modern suspension bridges. A space truss is built up from four chords connected by two vertical and two horizontal diagonal bracings. Section types (a) and (b) are typical sections for different deck widths if the traffic is to be carried only at the top level while in section (c) the sway bracing is substituted for a rigid frame which gives a solution for two level traffic capacity (Gimsing, 1998 p. 321-322). The stiffening girder of the Akashi Kaikyo Bridge is an example of a girder composed of three simply supported trusses.

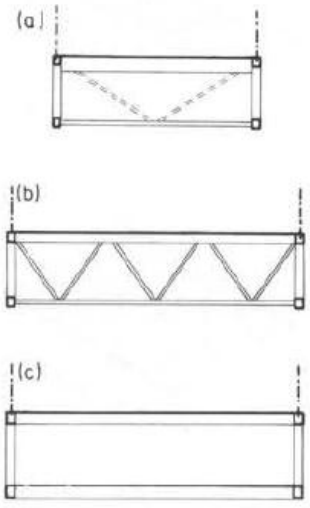

Figure 2-7: Basic truss girders (Gimsing, 1998)

Figure 2-8 shows different configurations of closed box girders organized in terms of aerodynamic properties. The top girder has a high drag coefficient of around 1,5 while with the semi streamlined cross section in the middle, it is possible to reduce the drag coefficient to below 1,0. The lowest section is more streamlined and includes web plates with small inclination to the wind direction and sharp edges to divide airflow which results in the possibility to decrease the drag coefficient to about 0,5. These characteristics significantly reduce fluttering of the girder. A streamlined box girder was first used in the Severn Bridge in the 1960s enabling a shallower girder than in the case of a truss and has since been applied in many bridges such as the Humber Bridge and the Great Belt East Bridge (Gimsing, 1998 p. 317-319). The longest box girder suspension bridge in the world is the Zhoushan Xihoumen Bridge in China which has a main span of 1650 m and currently ranks second of all suspension bridges behind the Akashi Kaikyo Bridge (Song & Dong, 2010).

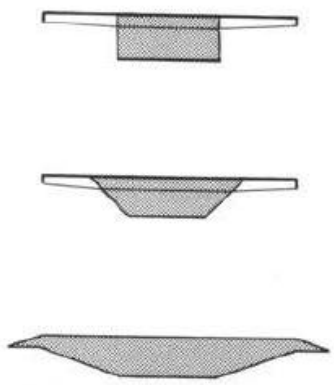

Figure 2-8: Box shaped girders (Gimsing, 1998)

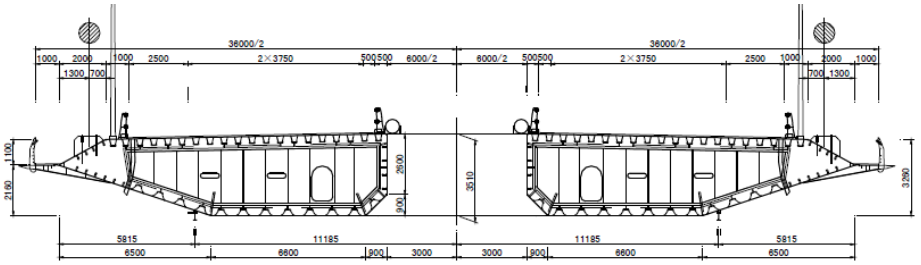

Figure 2-9: Box stiffening girder of the Zhoushan Xihoumen Bridge (Song & Dong, 2010)

Bridge deck

The bridge deck generally consists of a 200–300 mm thick concrete slab supported by floor beams in the longitudinal direction of 3000–5000 mm intervals, longer if prestressed or haunched. Steel decks, consisting of relatively thin deck plates which are stiffened by longitudinal ribs and transverse floor beams are also used but are likely to be more expensive than concrete decks. The lighter weight of steel is however likely to reduce construction costs of other structural parts such as cables, pylons and piers so all aspects of the superstructure have to be considered in the choice of materials. Composite construction involving a concrete slab and steel girder decking has also become quite common in recent years (Gimsing, 1998 p. 304-305).

2.2.2 Cables

The main cables serving as the main load bearing element in suspension bridges can have a diameter ranging from a few centimeters in short spans up to over a meter for long spans. These cables consist of steel wires usually of cylindrical shape with a diameter of 5-5,5 mm which are either laid out individually or in wire strands depending on the method of construction. The simplest strand used in cable supported bridges is the seven wire strand

which is normally made from seven 5 mm wires where a single straight wire core is surrounded by a layer of six wires, woven in helical format.

Figure 2-10: Seven wire strand

The high tensile strength of the steel wire makes it ideal for construction of suspension cables. The wires are cold drawn, giving a tensile strength of around 1570 MPa for individual wires which is approximately four times the strength of mild structural steel and twice that of high strength structural steel. Individual wires have a modulus of elasticity of about 205 GPa while the seven wire strands have about 190 GPa and tensile strengths between 1770 and 1860 MPa (Gimsing, 1998 p. 87-88).

Helical Strand Cables

Helical strands consist of multiple wires which are spun into layers of opposite direction around a straight core. Compared to the seven wire strand, the wires comprising the helical strand are further away from being straight thus decreasing the modulus of elasticity to around 170 GPa. This also reduces the strength to about 90% of the sum of the tensile strengths of the individual wires. Helical strands are subject to both elastic strain in the wires and inelastic strain due to compaction of the strand when loading is applied for the first time and are therefore pre-stretched before being put into service. Wrapping the wires together is unnecessary because of self-compacting characteristics due to the layers twisting around each other (Gimsing, 1998 p. 88-89). Helical strand cables are primarily used in bridges with shorter spans (Mayrbaurl & Camo, 2004).

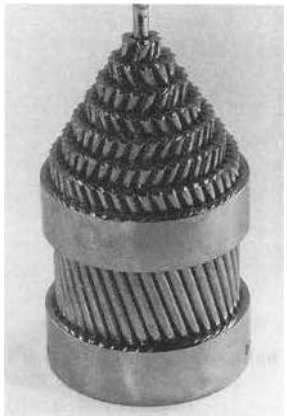

Figure 2-11: Helical strand (Gimsing, 1998)

Locked coil strands

Locked coil strands have a core of round wires similar to helical strands while the outer layers are of Z-shaped wires that interlock when stretched and therefore provide substantial protection for the inner layers. This reduces the need for corrosion protection and in most cases the only surface treatment of the galvanized wires is painting of the strand. The locked coil strand has a higher tolerance for transverse pressures at tower saddles and anchorages because of the larger contact surface of the Z-shaped wires. The modulus of elasticity is typically around 160 GPa (CEN, 2005) and similar to helical strands the tensile strength is about 90% of the strength of parallel wires. Locked coil strands are manufactured in full length and full cross section making it necessary to limit the diameters of long cables which are often in the range from 40 mm to 180 mm (Gimsing, 1998 p. 89-90). Because of the limitations of cable diameter, main cables of suspension bridges have

been constructed using groups of locked coil strands such as was done in the building of the Ölfusá Bridge.

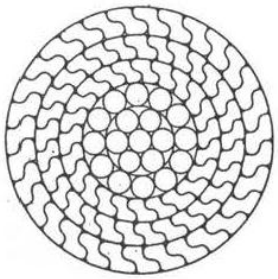

Figure 2-12: Cross section of a locked coil strand

Parallel wire strands

Laying out the individual wires parallel to each other is a solution which eliminates the need to reduce strength and stiffness of the strand due to twisting of the individual wires as needs to be done in the analysis of helical strand cables and locked coil strands. Parallel wire strands generally consist of 37, 61, 91 or 127 individual wires, assembled in a hexagonal pattern (Gimsing, 1998 p. 90-91).

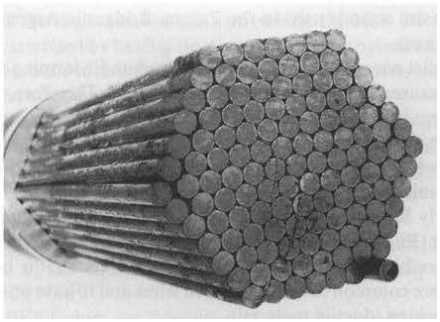

Figure 2-13: Parallel wire strand with 127 wires (Gimsing, 1998)

Parallel wire main cables

The main cables of intermediate and long span suspension bridges are constructed either by John Roebling´s air spinning method or the newer parallel wire strand method. The difference between the two methods is that in the air spinning method the wires are pulled between anchorages individually, while in the parallel wire strand method prefabricated strands are pulled across from one anchorage to the other. Each method has its advantages and disadvantages. The individual wires which are compacted into a circular shape after erection of all wires are easy to pull across but are unstable in windy conditions while the weight of the heavier and more stable strands can be a limiting factor (Gimsing, 1998 p. 98-99). For both the aerially spun- and prefabricated parallel wire strand methods, it must be ensured that all individual wire tensions are equal. This is done by making sure that all the wires sag equally during erection and is called the sag method (Mayrbaurl & Camo, 2004 p. 1.11).

2.2.3 Pylons

The vertical forces acting at the pylon top are very large. The pylon has to resist the weight of the bridge as well as the downward force that the anchorages exert on the cables. The vertical forces are transferred from the cable into the pylon by the pylon saddles which results in excessive normal pressures in the outer layer wires touching the surface of the saddle (Mayrbaurl & Camo, 2004 p. 1.12).

The critical loading on the suspension bridge pylon is as implied above, the axial force caused by the vertical components of the cables while in free standing tower structures the moment induced by wind is the most decisive load. The significance of the dead load depends on whether the pylon is constructed of steel or concrete. The lighter steel structure will experience much less increase of normal force from the pylon top to the base due to self-weight than a similar concrete structure. Factors such as soil conditions, speed of erection, stability in the construction period and of course cost will constitute the choice of material and despite the large self-weight of concrete pylons they are considered to be competitive for heights up to about 250 m (Gimsing, 1998 p. 345-346).

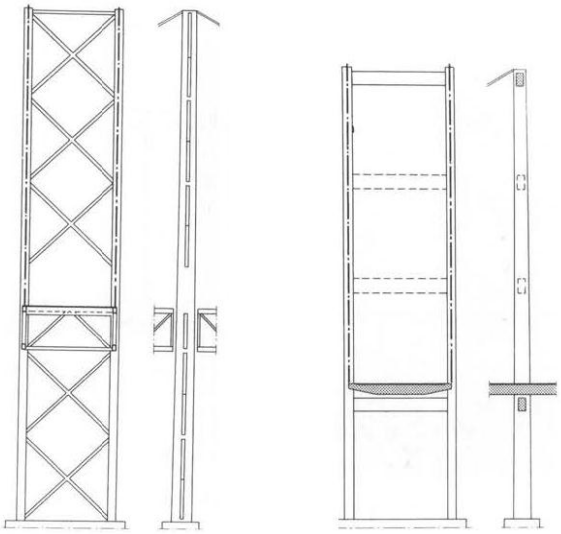

Figure 2-14: Left: Diagonally braced pylon. Right: Portal-type pylon

Figure 2-14 shows two common configurations of suspension bridge pylons. The diagonally braced pylon gives a high lateral rigidity acting as a vertical cantilevered truss and the portal frame pylon incorporates horizontal transverse beams rigidly connected between the main legs to provide adequate stiffness.

2.2.4 Main cable anchoring

To ensure adequate fastening of the main cables and safety of the superstructure, anchor blocks are constructed to transfer the force from the main cables to the soil. The large forces are distributed to the anchor block by using a splay saddle to separate the individual strands. This is shown in Figure 2-15. The separation of strands often takes place inside a splay chamber in the anchor block where, at the far end of the chamber, the strands are anchored to sockets which transfer forces into the concrete through steel bars. Also, post tensioned bars have proved as advantageous in transferring the strand forces to the concrete. To protect the individual strands from corrosion it has become common practice to install dehumidification systems in splay chambers (Gimsing, 1998 p. 402-406).

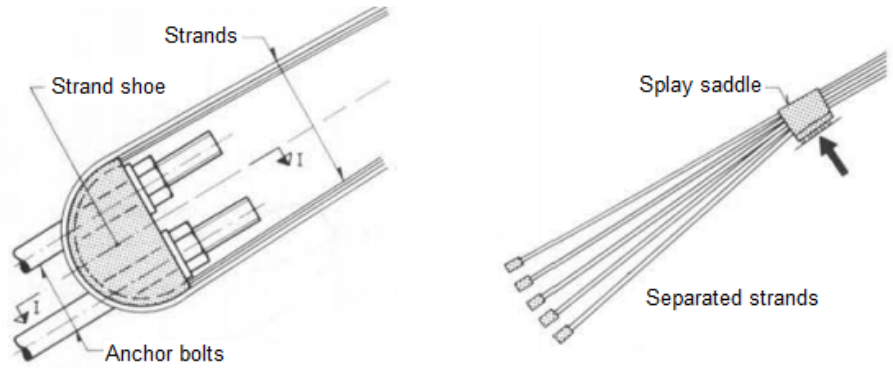

Figure 2-15: A strand shoe connecting separated strands to anchor block

Depending on the cable force, the construction of the anchor blocks tends to result in massive gravity structures such as the one in Figure 2-16. The anchor block needs to assure safe transmission of the horizontal and vertical component of the cable force by giving sufficient pressure at the foundation as well as provide stability against overturning. Both the weight of the structure and soil conditions are important factors affecting the design of the anchor block (Gimsing, 1998 p. 404-406).

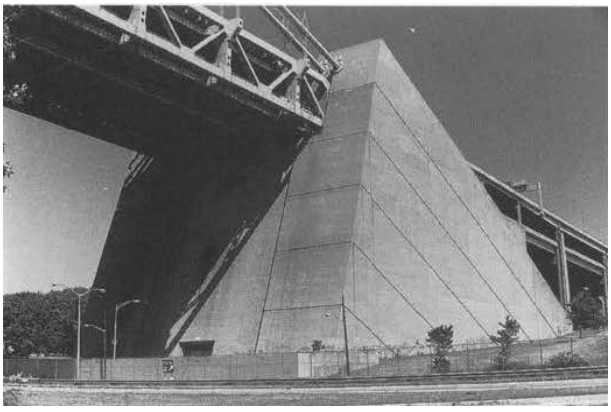

Figure 2-16: Anchor block of the 1298 m long Verrazano Narrows Bridge (Gimsing, 1998)

2.3 Loading conditions

The main loads affecting the design of suspension bridges are dead load, traffic load, wind load, seismic load, and temperature load. Other effects include corrosion, ice load, bridge scouring and occasional vessel collisions. The degree of importance of some load cases may be dependent on local environmental conditions and in particular projects, other types of loads such as erection load, impact load, and support movement may be considered.

2.3.1 Dead load

The dead load of a suspension bridge has a significant influence on the stiffness of the structure and often contributes most of the loading in design cases. The deformed equilibrium configuration of the stressed structural system is beneficial for further analysis such as initial conditions for dynamic analysis purposes. (Ren et al, 2004). The dead load includes the self-weight of all structural and non-structural members of the bridge, the self-weight of new coatings and earth cover. Also, the adding or removing of components should be taken into account (CEN, 2003a).

2.3.2 Railway and traffic load

Running trains induce vertical forces from the large vehicle weight, longitudinal forces from acceleration or braking, lateral forces caused by irregularities at the interface of the wheel and rail and centrifugal forces due to curvature of the track. Traffic running on bridges produces a stress spectrum which may cause fatigue. Traffic composition, axle loads, spacing between vehicles and dynamic effects are decisive factors for the significance of the stress spectrum. Fatigue load models are defined in Eurocode 1 (CEN, 2003b). Cars, buses, trucks and other heavy vehicles produce non-stationary loads on suspension bridges. Several parameters such as the axle loads, axle configuration, gross vehicle weight, number of vehicles, speed of vehicles and the bridge configuration influence the effect of highway loadings on suspension bridges (Xu & Xia, 2012 p. 16-17). Traffic load models are defined in Eurocode 1 (CEN, 2003b).

2.3.3 Wind load

Wind loading promotes instability and vibration, especially for long span suspension bridges and is therefore a major concern in design. Wind effects in the form of static forces are produced by mean winds, flutter instabilities, vortex shedding excitation, and buffeting excitation which is normally critical in determination of the size of structural members in long span suspension bridges. Design codes typically provide wind loads as a function of design wind velocity at a reference height above the ground or sea level but in the case of large scale suspension- and cable-stayed bridges, wind tunnel tests are often required to simulate the response of the bridge in various wind conditions (Xu & Xia, 2012 p. 18-19).

2.3.4 Seismic effects

Earthquake loads may be specified as horizontal effects given by the seismic base shear force which is the product of the elastic seismic response coefficient, the total mass of the

superstructure above the foundation and a correction factor. The elastic seismic response coefficient is adopted from a seismic design spectrum and is dependent on the fundamental period of vibration, ground acceleration determined from a regional contour map and soil conditions (CEN, 2003c). As the fundamental frequency of long span suspension bridges is generally low, seismic loading tends to be relatively small but should still be considered as an important factor (Xu & Xia, 2012 p. 19).

2.3.5 Temperature effects

Daily and seasonal variation in ambient temperature will cause deformation of bridge components. For long span suspension bridges in particular, temperature changes can have significant effects on deflections of the bridge deck and must be accounted for when deformations are measured. Due to the large potential deformations, induction of thermal stresses must be considered in the design process. The amplitude of temperature effects is dependent on the temperature distribution, structural configuration, boundary conditions and material characteristics (Xu & Xia, 2012 p. 18).

2.4 Suspension bridges in Iceland

The first major bridges of the Icelandic road system were suspension bridges at Ölfusá and Þjórsá built in 1891 and 1895 respectively. Today the road system comprises a total of seven suspension bridges, all built in the period from 1945-1967. The oldest one, carrying the largest amount of traffic is the Ölfusá Suspension Bridge which is also the only double lane suspension bridge. The other six are single lane bridges carrying less traffic (Guðmundsson, 2011a). Table 2-1 provides an overview of the bridges in chronological order.

Table 2-1: Suspension bridges (Icelandic Road Administration, 2011)

Bridge	Year built	Total Length [m]	Lane width [m]	AADT 2010	ASDT 2010
Ölfusá	1945	132,4	6,2	8462	10827
Jökulsá á Fjöllum	1947	102	3,7	305	609
Blanda	1951	72	3,8	105	179
Skjálfandafljót	1955	112	3,0	32	45
Jökulsá á Axarfirði	1957	116	3,8	395	668
Hvítá hjá Iðu	1957	107,4	3,8	462	686
Jökulsá á Breiðamerkursandi	1967	108,2	4,2	328	668

AADT: Average annual daily traffic
ASDT: Average summer daily traffic

3 Finite element model

This chapter presents a structural health monitoring oriented finite element model of the Ölfusá Suspension Bridge. The three dimensional model is constructed using the Sap 2000 commercial software (Computers and Structures, 2011) where cable, frame, solid, and shell elements are utilized. The intention is to model the structure as accurately as possible to provide a reliable basis for comparison with scheduled field tests. The field tests will among other things consist of ambient and forced vibration measurements which will provide information on the modal frequencies, damping properties and mode shapes of the bridge. With these parameters known, accurate dynamics-based calibration of the FE model and bridge characteristics may be obtained by fitting the FE model with the test data using model updating methods. Further objectives of this chapter include an evaluation of the altered structural responses induced by the installation of a heavier bridge deck in 1992 and a discussion on modal behavior with regard to potential accelerometer positioning in the scheduled vibration measurements.

The objective of this work is to supply reliable structural information that will be used for future health monitoring and preservation of the Ölfusá Bridge. As mentioned above, this chapter will address the modeling part of the investigation while tuning of the FE model and data processing after the field measurements in summer 2012 will be conducted by EFLA Consulting Engineers.

3.1 Bridge description

The Ölfusá Suspension Bridge, shown in Figure 3-1, is an important connection carrying highway 1 into the town of Selfoss, located about 10 km from Hveragerði and 57 km from Reykjavík. The bridge was built in 1945 and carries a two lane roadway over a cable supported main span of 84 m and three additional I-girder supported side spans. In 1992, a major renovation was undertaken where concrete damages in piers and anchor-blocks where fixed and the original 8 m wide concrete deck was replaced with a new 8,7 m wide concrete deck consisting of a 6,2 m wide roadway, a 1,8 m pedestrian lane and railings (Guðmundsson, 2011b).

Figure 3-1: Ölfusá Suspension Bridge

The replaced bridge deck caused a considerable increase to the self-weight of the structure and in combination with aging of the bridge and suspected degradation of the main cables it led to a visual evaluation in summer 2011 conducted by EFLA Consulting Engineers. In a following report, (Guðmundsson, 2011b), the main cable factor of safety was roughly estimated to be as low as 1,77 due to increase in self-weight and traffic load compared to about 4 at the time of construction in 1945. Despite this low factor, the estimation does not account for safety factors and deterioration of the cables and the favorable assumption is made that forces are equally distributed between cable planes.

The structural system of the suspension bridge is an earth anchored system and consists of a steel truss girder with a concrete deck on top, locked coil strand cables with suspenders over the main span, built-up steel section pylons and anchor-blocks.

The 84 m long stiffening girder has four longitudinal I-girders supporting the concrete deck and transferring deck loads to the steel truss which consists of three longitudinal trusses, and transverse trusses positioned at 4,0 m intervals. Two of the longitudinal trusses are vertical 1,496 m high on each side of the girder and one is a horizontal wind stiffening truss connected at the bottom of the girder. The transverse trusses, 1,496 m high at each end and 1,176 m high over the span are connected to the suspenders which transfer the bridge deck loads to the main cables. The two bottom chords of the vertical longitudinal trusses are 90 degree tilted I-girder sections with cover-plated flanges to increase stiffness.

Figure 3-2: Stiffening truss girder of the Ölfusá Bridge

The suspenders are made from circular steel sections and connect to the main cables at 4 m intervals of transverse trusses. The main cables are composed of 6 individual locked coil strands in each cable plane. Each strand is 60,1 mm in diameter and the distance between cable planes is 9,3 m. The tensile strength of each strand was estimated to be around 2650 kN at the time of construction. The strands of the main cables, opposed to strands in the majority of Icelandic suspension bridges, are not galvanized which makes them vulnerable to corrosion. The two sets of suspension cables are restrained by concrete anchorages on each side of the river. The east side anchor block is positioned 25 m away from the pylon centerline at an elevation of +14 m while the west side block is 18,5 m away from the centerline of the west side pylon at an elevation of +16,5 m. This layout results in similar angle of the two backstays but the elevation of the bridge deck and pylon tops is +18,2 m and +28,38 m, respectively.

Figure 3-3: Left: Main cables. Right: Pylons

The pylons rise about 10,2 m above the bridge deck giving maximum cable sag of 10,5 m at the middle of the span. The built-up steel section of the pylon consists of two I-girder sections connected by plates. The pylons transfer the vertical component of the main cable force to the foundations. A hinge at the bottom allows pivoting in the longitudinal direction, reducing bending moments in the section while the cables are clamped by a saddle at the top. The two pylons stand on concrete pier foundations; 6,4 m high on the east side of the river and 4,6 m high on the west side. Three additional concrete piers support the I-girder supported side spans on the east side of the river.

3.2 Modeling of the bridge

The three dimensional modeling of the bridge is conducted using CSI SAP2000 v15 for static and modal load cases and CSI Bridge v15 for moving load analysis. The model, shown in Figure 3-4, is used for both static nonlinear- and modal analyses. In addition to an on-site investigation, the model is constructed with help from both original design drawings from the Dorman Long Company that designed the bridge in 1945 and post-renovation drawings from 1992. The main focus during the modeling process was to represent the actual geometry as accurately as possible with careful placement of elements according to drawings, proper simulation and quantification of element mass and stiffness, and boundary conditions that represent real conditions. Also, the level of detail should be sufficient for subsequent model updating. Two versions of the model where created, one including the original bridge deck and another version with the larger deck from 1992.

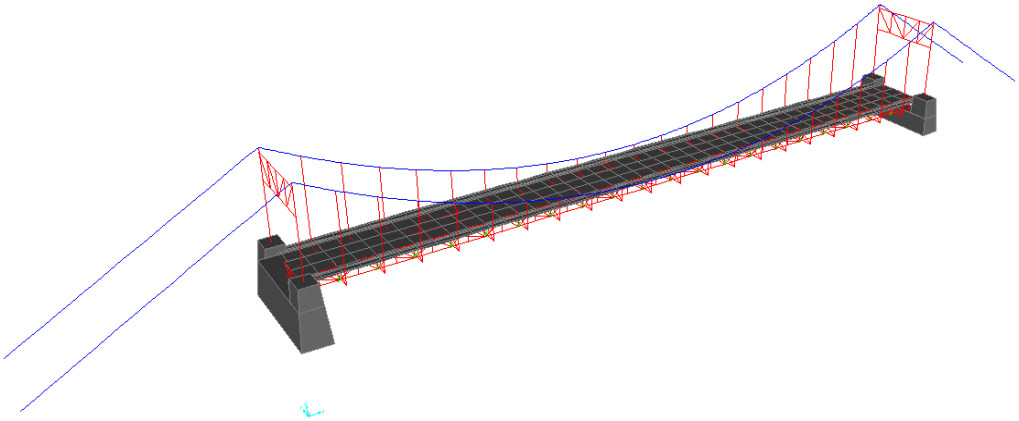

Figure 3-4: Finite element model of the Ölfusá Bridge

3.2.1 Truss girder and bridge deck

The suspended truss girder has a repetitive structural configuration at 4 m intervals over the main span. The four upper longitudinal chords that carry the bridge deck and the two 90 degree tilted lower chords (see Figure 3-5 and Figure 3-6) are I-beams modeled as 12-DOF frame elements with section properties given in Table 3-1. Vertical members and diagonals of the longitudinal trusses are angle sections summarized in Table 3-2 where the vertical double angles are adjacent to the transverse intermediate girders while the vertical single angles are positioned in between.

Table 3-1: Longitudinal I-girder section properties

	Section [in.]	**Plate [in.]**	**A [mm^2]**	**I_y [mm^4]**	**I_z [mm^4]**
Deck stringers (inner chords)	15" x 6" x 45#	-	7472	1,8E+08	8,7E+06
Top chord (outer, at ends)	14" x 8" x 40#	-	7924	1,8E+08	1,8E+07
Top chord (outer, over span)	14" x 8" x 40#	10x3/8 (web)	12750	2,1E+08	1,9E+07
Bottom chord	14" x 8" x 70#	-	12912	2,9E+08	3,2E+07
Bottom chord	14" x 8" x 70#	8x3/8 (flanges)	16788	4,2E+08	4,5E+07

Table 3-2: Longitudinal truss girder section properties

	Section [in.]	**$A_{section}$ [mm^2]**	**$I_{y,\ section}$ [mm^4]**	**$I_{z,\ section}$ [mm^4]**
Diagonals 0-4m from end	2L: 4" x 4" x 5/8"	5956	5,6E+06	1,4E+07
Diagonals 4-8m from end	2L: 4" x 4" x 1/2"	4838	4,6E+06	1,1E+07
Diagonals rest of span	2L: 4" x 4" x 3/8"	3680	3,6E+06	8,2E+06
Vertical angles 2,6,10m,...	L: 3" x 3" x 3/8"	1357	7,3E+05	7,3E+05
Vertical angles 4,8,12m,...	2L 3 1/2" x 2 1/2" x 3/8"	2660	2,1E+06	2,2E+06
Wind girder angle	L 4 1/2" x 4 1/2" x 3/8"	2060	2,6E+06	2,6E+06

Both the end cross trusses at the piers, and in-span cross trusses at 4 m intervals, shown in Figure 3-5 and Figure 3-6, are of angle sections; all modeled as double angles except the

middle cross bracing and diagonals connected to the suspenders which are single angle sections. The horizontal bottom wind bracing, which connects to every other cross truss, is also an angle section. Section properties of the transverse girders and wind bracing are given in Table 3-3, Table 3-4 and Table 3-2, respectively. The wind bracing and also the lower chord I-beams are positioned at the same elevation as the bottom of the end cross trusses and are thus connected to the in-span cross trusses by plated connections at joints.

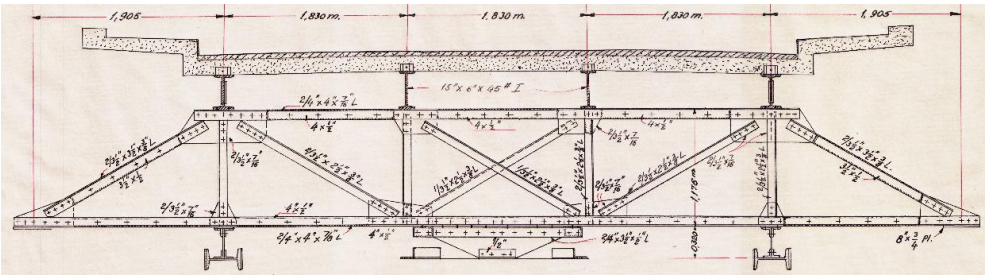

Figure 3-5: Original in-span cross section with 8,0 m wide deck

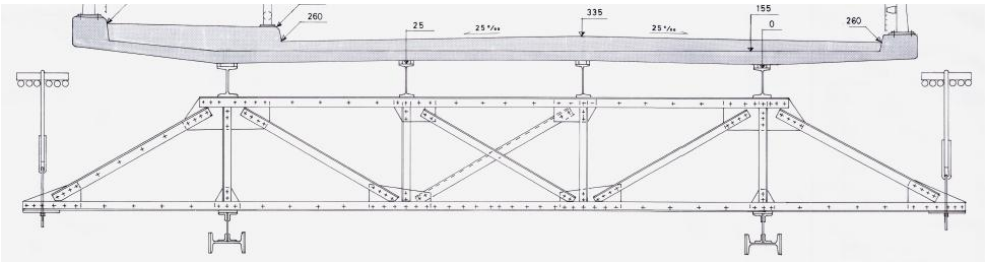

Figure 3-6 Current in-span cross section with 8,7 m wide deck

All truss members are modeled as 12-DOF continuous frame elements and meshed at intermediate joints, at intersections with other frames and area edges, and with a maximum length of segments of 2 m. All frame elements are connected at the center of mass cardinal point except the four upper longitudinal I-beam chords. Those are connected to the horizontal cross frame elements at their middle bottom cardinal points for correct representation of member elevations.

Table 3-3: Intermediate cross girder section properties

	Section [in.]	**Plate [in.]**	**$A_{section}$ [mm^2]**	**$I_{y,\ section}$ [mm^4]**	**$I_{z,\ section}$ [mm^4]**
Horizontal top angle	2L 4" x 4" x 7/16"	4" x 1/2"	4247	4,1E+06	9,4E+06
Horizontal bottom angle	2L: 4" x 4" x 7/8"	4" x 1/2"	8247	7,3E+06	2,2E+07
Diagonals (inner)	2L 3 1/2" x 2 1/2" x 3/8"	-	2660	2,1E+06	2,2E+06
Cross bracing (middle)	L 3 1/2" x 2 1/2" x 3/8"	-	1345	1,1E+06	4,5E+05
Diagonals (outer)	2L 3 1/2" x 3 1/2" x 3/8"	3 1/2" x 1/2"	3170	2,4E+06	5,6E+06
Vertical angles	2L 3 1/2" x 2 1/2" x 3/8"	-	2660	2,1E+06	2,2E+06

Table 3-4: End cross girder section properties

	Section [in.]	Plate [in.]	$A_{section}$ [mm^2]	$I_{y, section}$ [mm^4]	$I_{z, section}$ [mm^4]
Horizontal top angle	2L 3 1/2" x 3 1/2" x 3/8"	3 1/2" x 1/2"	3170	2,4E+06	5,6E+06
Horizontal bottom angle	2L 3 1/2" x 3 1/2" x 3/8"	3 1/2" x 1/2"	3170	2,4E+06	5,6E+06
Diagonals	2L 3 1/2" x 2 1/2" x 3/8"	-	2660	2,1E+06	2,2E+06
Cross bracing (middle)	L 3 1/2" x 2 1/2" x 3/8"	-	1345	1,1E+06	4,5E+05
Vertical angles	2L 3 1/2" x 3 1/2" x 3/8"	-	3170	2,4E+06	5,6E+06

Section properties that are automatically computed by the software are checked and modified according to values from the steel manufacturer Arcelor Steel (Arcelor, 2006), and the Historical Structural Steelwork Handbook (Bates, 1991). The density of steel structural members is taken as 8820 kg/m^3 (about 10% higher than normal steel density of 7850 kg/m^3) to account for the added weight of connections and rivets. The modulus of elasticity is taken as 200 GPa and Poisson´s ratio is 0,3.

The concrete bridge deck is modeled as thin shells using four node area elements with proper offsets and manipulation of thickness to exactly capture the stiffness and configuration of the deck. The density, modulus of elasticity, and Poisson´s ratio of the current deck are taken as 2500 kg/m^3, 32 GPa, and 0,2, respectively while reducing the concrete density of the original bridge deck. This modification is done with regard of weight comparison between design documents and model results whereas the objective is to capture the actual structural behavior as accurately as possible. The two types of deck plates modeled for analysis purposes where: Firstly, an 8,0 m wide plate representing the original bridge deck for comparison with deflection tests from 1946 and modal properties presented by Sigbjörnsson and Bessason (1982), where modal frequencies and shapes of the Ölfusá Bridge where calculated using analytical mode for suspension bridges. The deck plate is shown in Figure 3-5. Secondly, an 8,7 m wide plate representing the plate installed in 1992. This newer deck, shown in Figure 3-6, is of substantially larger construction than the original deck. It is installed in 1,205 m long, 0,1 m thick elements which are connected to the longitudinal I-beams by grouted stub connections, inducing composite effects. The plates carry the concrete road surface layer, including a sidewalk on one side of the roadway. The constructing of the sidewalk in 1992 is bound to have caused some disturbance in the equal force distribution between the cable planes and the exact modeling of the deck should simulate the effects from the altered distribution of weight. The area elements are connected to the supporting I-girders at the locations of the grouted stub connections with properly clarified offsets according to correct elevation of members in the attempt to capture composite effects between the deck and girders.

3.2.2 Cable system

The cable system of the bridge consists of the main cables, spaced 9,3 m apart, and suspender units, spaced at 4 m intervals over the main span. The main cables are composed of six individual locked coil strands in each cable plane (see Figure 3-3). Each group of strands is modeled as a single cable with modified sectional properties to a factor of 6 to imitate the whole group. According to design documents, the effective steel area of each

strand is 2176 mm^2. The main cables are modeled as nonlinear cable elements which take account of catenary behavior and tension stiffening using an elastic catenary formulation. The use of the cable element requires nonlinear geometry analysis to calculate large deformations under applied loading, whether in the form of self-weight, temperature or initial strain loading. The initial ordinates of the cable are found by forming a parabolic profile between the pylons with a maximum sag of 10,5 m at the middle of the span. The tensile strength of each strand is according to design documents, around 270 tons (2650 kN). For the whole group of strands, the strength in each cable plane is then F_{Rk} = 15900 kN which means a maximum stress value of 1218 MPa.

The suspenders are made from circular steel sections, two inches in diameter and are modeled as 12-DOF frame elements with all degrees of freedom fastened to provide stiff enough boundary conditions for the connected cable elements.

The density of the cables is taken as 8300 kg/m^3 (CEN, 2005) and Poisson´s ratio is 0,3. The modulus of elasticity is taken as 135 GPa which is an average of a value of 139 GPa from Dorman Long design documents (1945) and 131,5 GPa from hand calculations performed subsequent to load tests in 1946 (Pálsson, 1947). The suspenders are modeled with the same type of construction steel as the stiffening girder elements.

3.2.3 Pylons

The bridge pylons which are made from two I-girder sections connected by steel plates and filled with concrete are modeled as custom made 12-DOF frame elements (see Figure 3-7). The I-girders are of 24" x 7 1/2" 95# sections and the flange plates are 28" by 15/16". At the bottom support, five degrees of freedom are continuously connected to the bridge pier, enabling only rotational movement in the longitudinal direction of the bridge to simulate the hinge effects (see hinge in Figure 3-3). A wind bracing of angle sections connects the two pylons at the top, increasing out of plane stability of the structure. Both the angle sections and the steel of the custom designed pylon section have a scaled mass density of 8820 kg/m^3, modulus of elasticity of 200 GPa and a Poisson´s ratio of 0,3. The concrete fill has a density, modulus of elasticity and Poisson´s ratio of 2500 kg/m^3, 32 GPa and 0,2, respectively.

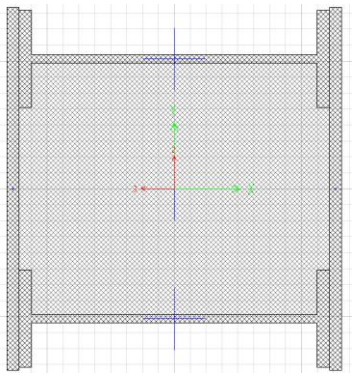

Figure 3-7: Pylon section

3.2.4 Connections and supports

Accurate modeling of the connection between the main cables and anchor block is very difficult since the main cable strands are led through a clamp splitting the strands to distribute the cable tension evenly into the block. The anchorages themselves are therefore not included in the model, whereas fixed supports are assigned at the main cable ends. The tower saddles, leading the main cables over the pylon tops are considered as being sufficiently stiff allowing for the cables to be modeled as fixed over saddles.

Due to the height difference between the longitudinal truss and intermediate cross truss over the main span (see bottom of Figure 3-6), the bottom angle section of the intermediate cross truss is elevated at +16,435 m while the bottom chord of the longitudinal truss runs at an elevation of +16,115 m. A rigid link is used for modeling this 320 mm high connection which in the actual structure consists of a massive plate fastened to the adjacent members by rivets. Rigid links are also used for the connection between the horizontal bottom wind girder and cross girders.

The end cross girders connect to the piers at the ends of the bottom chord I-girders and also in the middle where the wind girder connects to the pier through a connection transferring the wind induced forces into the pier. At the east side of the span, all three translational degrees of freedom are fastened while some movement in the longitudinal direction is accounted for at the west side. The concrete piers are modeled according to design drawings as solid elements with fixed bottom supports. The mass density, the Poisson´s ratio, and the modulus of elasticity of the reinforced concrete of the piers is estimated to be 2500 kg/m^3, 0,2, and 32 GPa, respectively.

3.2.5 Non-structural elements

The weight of non-structural elements affecting the bridge mass are modeled in the form of applied loading. Some deviations are made between the original and present configuration of the bridge in terms of loading. The thickness of roadway asphalt is documented as 5 cm in original design documents, modeled with the mass density of asphalt taken as 2200 kg/m^3 while the newer construction does not have an asphalt surface. The asphalt loading on the older construction is assigned as uniform load on the shells comprising the highway lanes. The weight of the parapets is taken from design documents. The same weight is assumed for the inner railing of the newer deck although it is made from aluminum posts. The IPE-140 beams, supporting the gondola and pipelines under the bridge deck are only included in the modeling of the present configuration. The weight of the six pipes, calculated by taking the pipes as filled with water, results in considerable loading. The weight of the parapets, beams and pipelines are assigned to the model as point loads distributed at constant interval in the longitudinal direction of the bridge. The weight of structural and non-structural components is summarized in Table 3-13 of section 3.5.

3.3 Theoretical background

Suspension bridges are complex structures and to ensure safe and economic design, in combination with enhancement in construction techniques, accurate and reliable analysis methods are of most importance. The analysis methods used for suspension bridges can be divided into two categories of analytical and numerical types as described by Kim and Thai (2011): Elastic theory and deflection theory are the basis of the analytical method. The stiffening effect of the main cable under tension is not accounted for in the elastic theory which results in higher moments in the stiffening girder. The deflection theory, first put into practice in design of the Manhattan Bridge, does consider second-order effects of cable stiffness, reducing the moments in the stiffening girder. With increased focus on accurately modeling more complex structural configurations, the numerical method is considered to

provide a more precise prediction than classical analytical methods of the response of suspension bridges.

This section addresses the methods used for analysis of the Ölfusá Bridge based on the three-dimensional finite element model. A brief description of geometric nonlinearity is given and the fundamentals of dynamic theory, necessary for the application of modal analysis are explained with reference to calculation procedures employed in the Sap 2000 software. Finally, a discussion describing the numerical solution techniques of the finite element method follows.

3.3.1 Nonlinear static analysis

Geometric nonlinearity

Nonlinearity in structural analysis can be caused by either geometric or material nonlinearity or in some cases both. The former arises when a structure is subjected to such large deformations that considerable alteration occurs in load application and resistance. The latter accounts for a nonlinear stress-strain relation in the structural material under applied loading (Cook, 1995).

In contrast to nonlinear response, linear response of structures is directly proportional to load. Displacements and rotations are assumed to be small, settling of supports is not accounted for and the stress-strain relationship is directly proportional. No directional changes of loading occur due to deformation of the structure, equilibrium equations are written with reference to original support conditions and displacements can be calculated in a single step of calculations. With larger displacements and rotations, the assumption of proportionality in the relationship between load and response ceases to accurately describe the structural behavior so the equilibrium equations need to be written for the deformed shape of the structure rather than the original configuration. Also, large rotations may cause a change in direction and magnitude of loads (Cook, 1995). A problem involving a structure encountering such effects may require nonlinear forms of analysis with iterative calculation procedures to yield adequate results.

SAP2000 has two ways of considering geometric nonlinearity, either in the form of P-delta effects or P-delta plus large-displacement/rotation effects assuming small strains within elements in both cases. Geometric nonlinearity may be taken into account on a step-by-step basis in nonlinear static and direct-integration time-history analysis. The stiffness matrix resulting from these solution methods can then be used for subsequent linear analyses (Computers and Structures, 2011).

In the modeling of the Ölfusá Bridge, geometric nonlinearity is taken into account in the form of P-delta plus large displacement effects, solved by nonlinear static analysis.

P-Delta and large displacement effects

P-delta type of nonlinearity takes partially account of the deformed configuration of the structure while iteratively solving the equilibrium equations. Geometric stiffening of the structure occurs when tensile forces reduce the rotation of elements while compressive forces tend to cause instability with enhanced rotation of elements. Large displacement type of nonlinearity considers a fully deformed configuration, also accounting for rotations,

when solving the equilibrium equations demanding a larger amount of iteration. For some cable supported structures, the application of P-delta analysis is sufficient unless significant deflection or rotation of the supporting structure, or the structure supported by the cables is expected. Large displacement effects are though recommended for analysis of models utilizing cable elements (Computers and Structures, 2011).

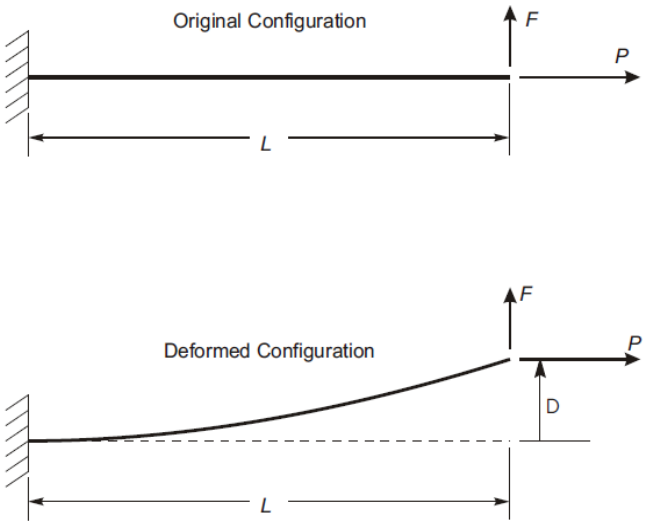

Figure 3-8: P-delta effects in a cantilever beam (Computers and Structures, 2011)

Figure 3-8 shows an example of a cantilever beam subject to an axial load *P* and a transverse load *F* at the tip, illustrating the concepts behind the P-delta effect. Considering the original configuration of un-deformed geometry, the moment at the support is *M=FL* and decreases linearly to zero at the tip. In the case of a deformed configuration, additional moment is caused by the axial force *P*, acting on the transverse displacement at the tip, *D*. Linear moment distribution along the length of the beam no longer exists but instead, the distribution depends upon the deflected shape giving a moment *M=FL-PD* at the support. This example illustrates the moment reducing effects of a beam in tension, increasing geometrical stiffness against the transverse load *F*. For a beam under compressive loading however, the moment and transverse bending are increased, causing a greater flexibility against the load *F* which eventually will lead to buckling of the member.

The magnitude of P-delta effects is illustrated by Wilson (2002) where it is noted that if the weight of a structure is large in proportion to the lateral stiffness, the contributions of the P-delta effects are highly amplified and may cause an increase of twenty five percent or more in the displacements and member forces. The analysis of a structure subjected to excessive P-delta effects will eventually encounter singularities in the solution indicating instability of the structure and need for additional stiffness.

3.3.2 Equations of motion

Dynamic analysis of multiple degree of freedom structural systems is a direct extension of static analysis. Inertia forces and energy dissipation forces just need to be incorporated to provide satisfactory dynamic equilibrium and the mass of the structure has to be lumped at the joints. The elastic stiffness matrices remain unchanged (Wilson, 2002).

The response of a structure subjected to external dynamic excitation may be described by formulation of the equations of motion for an idealized multiple degree of freedom system. The methodology can be explained by a two story frame of completely rigid floors, subjected to external forces $p_1(t)$ and $p_2(t)$ (see Figure 3-9).

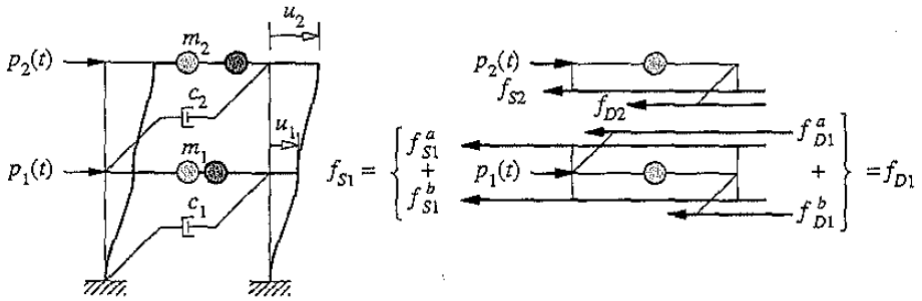

Figure 3-9: Two story shear frame and acting forces (Chopra, 2007)

The figure shows the forces acting on each floor mass *m*. These forces are the external force *p(t)*, the resisting force f_s and the damping force f_D. The lateral displacements and damping of the system are represented with *u* and *c*, respectively. Newton´s second law of motion may be used to express the equilibrium of the frame floor masses, written in matrix form (Chopra, 2007).

$$\begin{bmatrix} m_1 & 0 \\ 0 & m_2 \end{bmatrix} \begin{Bmatrix} \ddot{u}_1 \\ \ddot{u}_2 \end{Bmatrix} + \begin{Bmatrix} f_{D1} \\ f_{D2} \end{Bmatrix} + \begin{Bmatrix} f_{S1} \\ f_{S2} \end{Bmatrix} = \begin{Bmatrix} p_1(t) \\ p_2(t) \end{Bmatrix} \qquad [3.1]$$

In compact form, the equation of motion can be written as

$$[M]\{\ddot{u}\} + \{f_D\} + \{f_S\} = \{p(t)\} \qquad [3.2]$$

Where *[M]* is the mass matrix of the frame, $\{\ddot{u}\}$, *{f_D}*, *{f_S}* and *{p(t)}* are the vectors of acceleration, damping force, resisting force, and external excitation, respectively.

By incorporating the full stiffness, *k*, of each story, a relationship between the elastic resisting force vector *{f_S}* and the displacement vector *{u}* can be obtained through the stiffness matrix *[K]* as

$$\begin{Bmatrix} f_{S1} \\ f_{S2} \end{Bmatrix} = \begin{bmatrix} k_1 + k_2 & -k_2 \\ -k_2 & k_2 \end{bmatrix} \begin{Bmatrix} u_1 \\ u_2 \end{Bmatrix} \qquad [3.3]$$

This can be written in compact form as

$$\{f_S\} = [K]\{u\} \qquad [3.4]$$

The damping forces are related to the floor velocities $\dot{u}_1$ and $\dot{u}_2$, and can be expressed in a similar manner, written in matrix- and compact form as

$$\begin{Bmatrix} f_{D1} \\ f_{D2} \end{Bmatrix} = \begin{bmatrix} c_1 + c_2 & -c_2 \\ -c_2 & c_2 \end{bmatrix} \begin{Bmatrix} \dot{u}_1 \\ \dot{u}_2 \end{Bmatrix} \quad [3.5]$$

and

$$\{f_D\} = [C]\{\dot{u}\} \quad [3.6]$$

By substitution of equations [3.4] and [3.6] into [3.2], a set of ordinary differential equations governing the displacements of the two story frame can be written as

$$[M]\{\ddot{u}\} + [C]\{\dot{u}\} + [K]\{u\} = \{p(t)\} \quad [3.7]$$

This matrix equation describes a system subjected to external dynamic forces and can be expanded for a structure of any number of degrees of freedom. In the case of a structure that does not experience external excitation the equation is reduced to describe the behavior of a freely vibrating structure.

3.3.3 Modal identification

Random loading such as wind and human induced loads provide a continuous state of dynamic motion in structures. These small ambient vibrations tend to be in the vicinity of the natural frequencies of the structure and its energy is absorbed by energy dissipation of the structural system. At any time, the displaced shape *{u}* may be a natural mode shape or any combination of the natural mode shapes of the system. By performing ambient vibration measurements of the structure its natural periods and modes can be computed and compared to results of computer models (Wilson, 2002).

The free vibration of an undamped system is described with the following second order homogeneous differential equation (Chopra, 2007).

$$[M]\{\ddot{u}\} + [K]\{u\} = \{0\} \quad [3.8]$$

The initial conditions at the time *t=0,* giving rise to the free vibration of the system are

$$u = u(0) \qquad \dot{u} = \dot{u}(0) \quad [3.9]$$

If the assumption is made that the structure vibrates in a simple harmonic motion, the displacement may be written as

$$\{u\} = q_n(t)\{\phi\} \quad [3.10]$$

where *{ϕ}* is a mode shape of free vibration, independent of time, and $q_n(t)$ is the time dependent alteration of the displacements, expressed by the simple harmonic function

$$q_n(t) = A_n \cos \omega_n t + B_n \sin \omega_n t \quad [3.11]$$

where A_n and B_n are arbitrary constants of integration and ω_n is the circular frequency (radians/second) of free vibration. Inserting equation [3.11] into [3.10] gives the displacement as

$$\{u\} = \{\phi\}\left(A_n \cos \omega_n t + B_n \sin \omega_n t\right) \qquad [3.12]$$

By differentiating the displacement twice with respect to time, the accelerations are obtained and then substituted into equation [3.8]. This yields the equation

$$\left([K] - \omega_n{}^2 [M]\right)\{\phi\} = \{0\} \qquad [3.13]$$

The solution, *{ϕ}={0}*, implying no motion of the system, is trivial and therefore omitted. The non-trivial solution of [3.13] leads to the following problem stated for determination of the unknown natural frequencies, ω_n expressed as scalars and natural modes, *{ϕ}* written in vector form.

$$\det\left([K] - \omega_n{}^2 [M]\right) = 0 \qquad [3.14]$$

This equation is called the characteristic equation of motion or frequency equation. The *N* roots, $\omega_n{}^2$, of the equation determine the *N* natural frequencies ω_n of vibration *(n=1,2,…,N)*. These roots are known as eigenvalues and when a natural frequency ω_n is known, equation [3.13] can be solved to yield a corresponding vector of natural mode shape of vibration *{ϕ}*. These vectors are known as eigenvectors, containing relative values of the *N* displacements of an *N*-degree of freedom system. Each frequency ω_n of the system corresponds to a natural period T_n and a natural mode *{ϕ}* which are related to the natural frequency f_n by

$$T_n = \frac{1}{f_n} \qquad \text{and} \qquad \mathrm{f}_n = \frac{\omega_n}{2\pi} \qquad [3.15]$$

The *N* frequencies are arranged in ascending order:

$$\omega_1 < \omega_2 < \ldots < \omega_N \qquad [3.16]$$

The eigenvectors can be assembled into an *NxN* matrix where each column is a natural mode of the system and each line of the matrix represents a degree of freedom. This matrix is called the modal matrix:

$$\Phi = \begin{bmatrix} \phi_{11} & \phi_{12} & \cdots & \phi_{1N} \\ \phi_{21} & \phi_{22} & \cdots & \phi_{2N} \\ \vdots & \vdots & \ddots & \vdots \\ \phi_{N1} & \phi_{N2} & \cdots & \phi_{NN} \end{bmatrix} \qquad [3.17]$$

The spectral matrix Ω^2 contains the *N* eigenvalues, $\omega_n{}^2$:

$$\Omega^2 = \begin{bmatrix} \omega_1^2 & & & \\ & \omega_2^2 & & \\ & & \ddots & \\ & & & \omega_N^2 \end{bmatrix} \quad [3.18]$$

SAP2000 offers two types of modal analysis; eigenvector- and Ritz-vector analysis (Computers and Structures, 2011). For the definition of load cases for modal analysis of the Ölfusá Bridge, eigenvector analysis, as described above, is chosen to determine the undamped free vibration mode shapes and frequencies of the system. The modal analysis itself is always linear but can either be based on the stiffness of the unstressed structure, or upon the stiffness at the end of a nonlinear load case. The modal analysis conducted in this thesis is based upon the stiffness at the end of a nonlinear static analysis for evaluation of the modes under P-delta large displacement effects.

3.3.4 Finite element analysis

The finite element method is a numerical procedure that provides approximate results for problems that are too complicated to be accurately solved by classical analytical methods. In general, the method models a structure as a finite number of assembled elements, each of simple geometry and therefore easier to analyze than the full size structure. These assembled parts of the structure comprise a mesh of elements which is represented by a system of algebraic equations to be solved for unknowns at the element nodes. These equations are interpolation functions, adapted to the number of nodes in the element type (Cook et al., 2002).

The formulation of element matrices used for solving the global equations of the structure may be described, starting with interpolation of the displacements *{u}* over an element:

$$\{u\} = [N]\{d\} \quad [3.19]$$

Where N_i is a shape or interpolation function and *{d}* are the nodal deformations (displacements and rotations of the element. Determination of acting strains is given as:

$$\{\varepsilon\} = [B]\{d\} \quad [3.20]$$

The matrix *[B]* is called the strain-displacement matrix and from equations [3.19] and [3.20], the virtual displacement *{δu}* and strain vector *{δε}* can be expressed:

$$\{\delta u\}^T = \{\delta d\}^T [N]^T \quad \text{and} \quad \{\delta\varepsilon\}^T = \{\delta d\}^T [B]^T \quad [3.21]$$

By the use of general stress-strain relations, the principle of virtual work, and equations [3.20] and [3.21], a relationship describing the behavior of the local element may be obtained and simplified into the following equation:

$$[k']\{d\} = \{r_e\} \quad [3.22]$$

Where $\{r_e\}$ is the vector of loads applied to element nodes and *[k´]* the element stiffness matrix given as:

$$[k'] = \int [B]^T [E][B] dV \quad [3.23]$$

Where *[E]* is the constitutive matrix of elastic constants. Equation [3.22] yields the element stiffness matrices in local coordinate system which are then transferred to global coordinates of the structure by using the transformation matrix *[T]*:

$$[k] = [T]^T [k'][T] \quad [3.24]$$

When transformation into global coordinates has taken place, the elements are assembled to form a finite element structure. That is, element matrices are expanded to represent the whole structure resulting in the structure or system equilibrium equations

$$[K]\{D\} = \{R\} \quad [3.25]$$

with *[K]* denoted in section 3.3.2 as the stiffness matrix of the structure, *{D}* is the global vector of degrees of freedom and *{R}* is the vector of external loads that are applied at structure nodes.

For a more thorough explanation of the formation of matrices for different types of elements, interpolation functions, and the application of finite element analysis, a reference is made to (Cook et al., 2002).

3.4 Computational results

This section summarizes the results obtained from the analytical model of the Ölfusá Suspension Bridge. The main objective is to describe both static and dynamic behavior of the structure in terms of deflections, section forces and identification of mode shapes. Two models were analyzed, the one representing the structure with the original bridge deck and the other one where the heavier deck installed in 1992 was modeled. For verification purposes of the finite element model, deflections are compared to load tests conducted in 1946 and also the modal periods of the first model are compared to results presented by Sigbjörnsson and Bessason (1982). This comparison is given in section 3.4.1 while section 3.4.2 focuses on the current state of the bridge. Based on the modal shapes analyzed in that section, an example of suitable accelerometer placement during scheduled dynamic tests will be given in the summary of this chapter.

3.4.1 Response of the original structural configuration

Static analysis

The main purpose of modeling the original configuration of the bridge is to validate the accuracy of the modeling process by comparing with documented test results and reaction forces from design drawings, both retrieved at the Icelandic Road Administration.

According to design drawings from the contractor Dorman Long, the suspension bridge cables were prestressed to 43 tons (UK) to mark the positioning of hanger clips for accurate cable sag once constructed. This is reported in load test documents from 1946 to have resulted in the bridge deck hogging to a height of +147 mm at the middle, above horizontal under dead load conditions. To achieve the correct amount of hogging effect of the bridge model, cable elements where subjected to strain loading, summarized in Table 3-5.

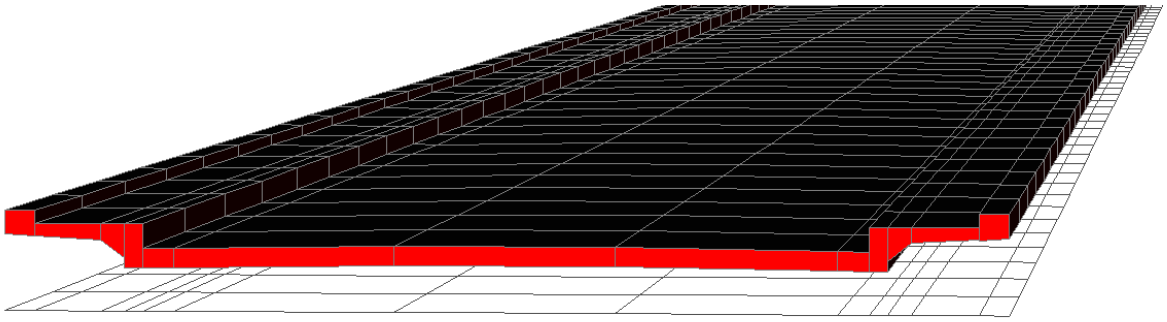

Figure 3-10: Extruded model view of the original bridge deck

The total reaction forces resulting from the weight of the main span and full length of cables are as follows:

Model Results = Design values=4718 kN

The reaction forces from the model results are calculated excluding the dead weight of the piers and pylons and should therefore be comparable with available design forces from Dorman Long. The resulting uniformly distributed loading can then be calculated as:

Model Results = Design values=4718kN/84m=56,2 kN/m

Table 3-5: Influence of cable pre-strain on deflections (δ) and axial forces (F) at mid-span

Prestrain	**Deflection[1,2]**	**Main cable**	**Suspenders**	**Top chord**	**Bottom chord**
[‰]	**δ [mm]**	**F [kN]**	**F [kN]**	**F [kN]**	**F [kN]**
0,00	-267	1807	83	13	2135
1,00	-84	2136	94	-4	690
1,50	8	2306	104	-10	-36
1,90	82	2445	109	-16	-619
2,10	118	2515	112	-19	-911
2,25	**147**	**2568**	**114**	**-24**	**-1130**
2,40	174	2622	116	-22	-1350

[1)]Deflection measured in stiffening truss bottom chord
[2)]Minus sign means down and plus up

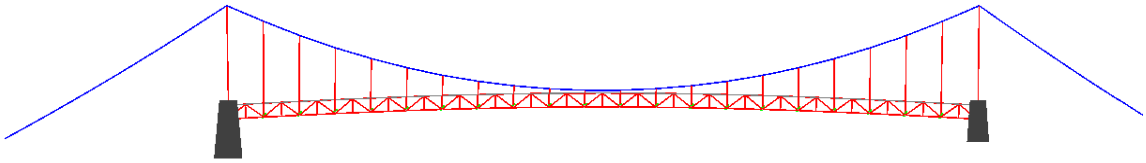

Figure 3-11: Deflected shape under dead load conditions (scaled)

Table 3-5 shows that an initial cable strain of 2,25‰ gives a mid-span deflection of +147 mm up and a maximum horizontal cable force of 2568 kN in each cable while the maximum cable force of 3057 kN occurs at the top of the west backstay. This gives a maximum cable stress of 234 MPa. The 2,25‰ value of strain will be considered to adequately describe the actual behavior of the bridge, resulting in values fairly close to the measured deflection of +147 mm and the design horizontal cable force of 2357 kN. This initial cable strain is therefore used in the following load test comparison, shown in Table 3-6. The testing of the bridge in December 1946 was carried out by transporting sand onto the bridge and measuring the resulting deflection at the middle of the 84 m long span. In the first test, 57,6 tons of sand where evenly distributed over a length of 30 m about the middle axis of the main span. Similarly in the second and third test, 96 and 14,4 tons where distributed over lengths of 50 and 8 m respectively. In the fourth test, a wagon of 4,9 tons was placed at the middle of the span.

Table 3-6: Comparison to load test from 1946

		Test 1	**Test 2**	**Test 3**	**Test 4**
Load length over midspan	[m]	30	50	8	(point load)
Loaded area	[m^2]	165	275	44	7
Load	[kN]	565	942	141	48
Test deflection, δ_T	[mm]	-43	-68	-8	-2
Model deflection, δ_c	[mm]	-55	-78	-15	-5
Difference	**[%]**	**22%**	**13%**	**47%**	**165%**

The test and model deflections compared in Table 3-6 may along with comparison of the cable force be the most accurate indicator of the validity and reliability of the computer model. Comparison of the first and second test yields a difference of 22% and 13% respectively. This gives an indication that the model is capable of adequately describing the actual structural behavior of the superstructure under evenly distributed loading over a large area at a global level. The third and fourth tests where deflections of significantly smaller values are compared are not as coherent but these values are likely to be more dependent on the local behavior of the structure because of the very small area of load distribution. Bearing in mind that actual behavior of single elements in a large scale global model is prone to be difficult to interpret and that the deflections of the third and fourth tests yield very small values, tests one and two may be regarded as a more adequate indicator of the accuracy of the finite element model. It should nevertheless be kept in mind that the FE-model gives systematically higher deflections than the field tests.

Modal analysis

The dynamic part of the original bridge configuration analysis focuses on the identification of mode shapes and their natural periods for comparison with theoretical calculations from 1982. A criterion of a minimum of ≈0,5% directional participating mass ratio is set to systematically separate the mode shapes of the finite element model according to directional and rotational properties. The shapes are then lined up according to the mode numbers of the 1982 calculations in Table 3-7. This investigation is not necessarily intended for further validation of the model, but rather for educational purposes whereas the main assumptions made are somewhat different and the two models being compared are of different nature. The former is an equivalent beam type of model while the latter is a hybrid model assembled with different kinds of elements capturing also the local responses of some critical members.

The dynamic analysis is conducted using the model of the original bridge configuration with the different modulus of elasticity of 190 GPa, differentiating from the properties yielding the static analysis results given in Table 3-5 and Table 3-6 where the modulus was taken as 135 GPa. This adjustment is made to imitate the settings assumed in the 1982 report as fairly as possible. According to Eurocode 8 (CEN, 2003c), the stiffness of the concrete deck used for modal analysis is taken as fifty percent of the uncracked stiffness due to the omission of an accurate analysis of cracked elements.

Table 3-7: Comparison of natural periods

1982 report		**Model results**				
Mode nr	**Period, T [s]**	**Mode nr**	**Period, T [s]**	**Difference**	***Shape**	
1	0,808	2	0,705	13%	Transverse	S
2	0,803	3	0,599	25%	Vertical	A
3	0,776	1	0,844	8%	Vertical	S
4	0,676	5	0,476	30%	Transverse	S
5	0,423	53	0,161	62%	Transverse	A
6	0,417	14	0,314	25%	Transverse	S
7	0,361	13	0,323	10%	Vertical	S
8	0,242	60	0,147	39%	Transverse	A
9	0,239	17	0,276	13%	Transverse	S
10	0,208	23	0,258	19%	Vertical	A
11	0,197	64	0,141	28%	Transverse	A
12	0,153	83	0,113	26%	Transverse	A

*S=symmetric, A=Asymmetric

As may have been expected from the discussion above, Table 3-7 reveals a considerable difference between the two methods of mode shape identification. However, the results are fairly consistent producing a difference of about 30% or less for all mode shapes apart from two of them. Furthermore, shapes nr 2 and nr 1 of the model results which are dominating in terms of participating mass ratios of 71% and 68% in the transverse and vertical directions, respectively are relatively coherent with the original calculations. The natural periods of these two critical shapes are only 13% and 8% off from original values indicating some similarity in terms of interpretation of the structural system. Given these results it should be noted that torsional modes were skipped in the 1982 report and are

therefore omitted from these model results. With that in mind, most of the intermediate mode shapes from the finite element model not passing the minimum participation mass criterion and are not given in Table 3-7 are either torsional shapes or shapes mainly expressing cable behavior. The following figures show the first three mode shapes from the finite element model.

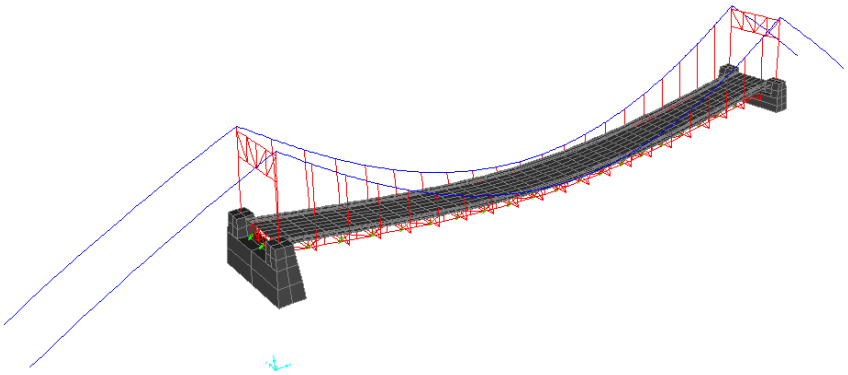

Figure 3-12: Mode 1, T=0,844s - 1st vertical mode shape (original bridge configuration)

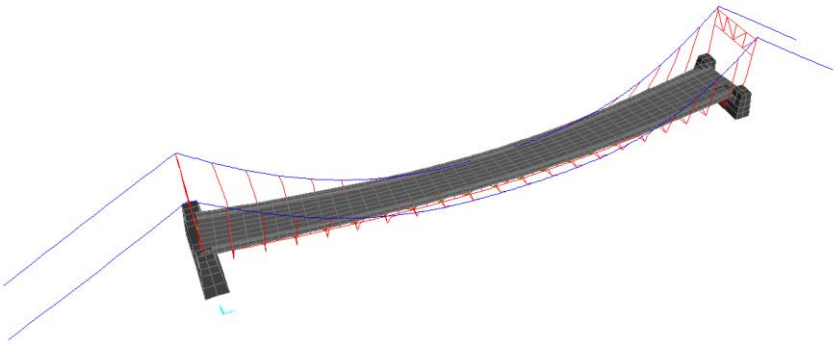

Figure 3-13: Mode 2, T=0,705s - 1st transverse mode shape (original bridge configuration)

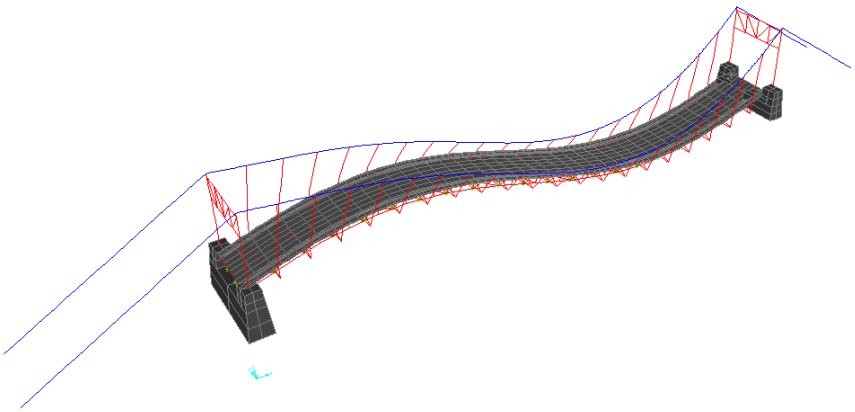

Figure 3-14: Mode 3, T=0,599s - 2nd vertical mode shape, (original bridge configuration)

3.4.2 Response of the current structural configuration

Static analysis

After installation of the new and heavier bridge deck in 1992, the bearing elements of the bridge were subjected to a significant increase in loading. Furthermore, the new deck is not symmetric about the longitudinal axis of the bridge, causing possible differences in force distribution between cable planes, not accounted for in the original design of the bridge. Visual inspection of the vertical layout of the present bridge deck implies that the deck is in a nearly horizontal position. The documented measurements, explained in section 3.4.1 where the level of the middle of the span was measured at +147 mm above horizontal, then suggest that the increased self-weight has enforced considerable deformations in the structural system.

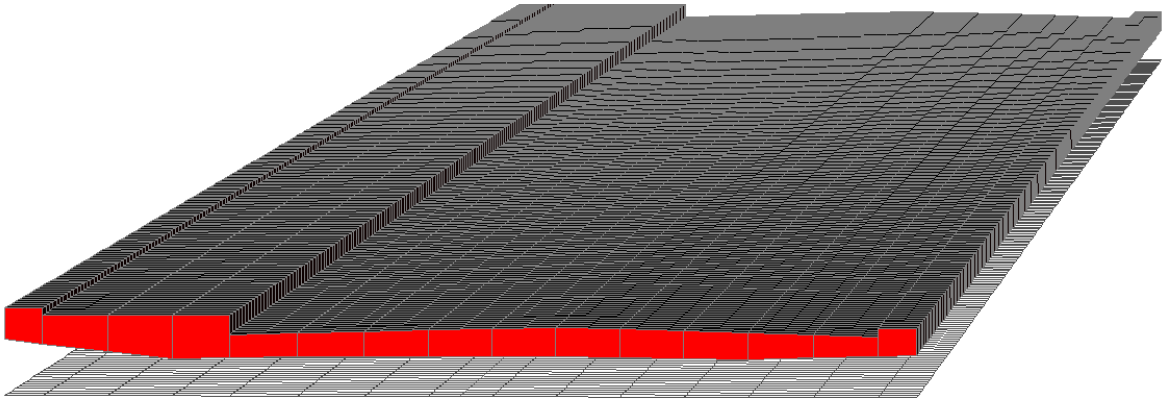

Figure 3-15: Extruded model view of the current bridge deck

The load test and cable force comparison of documented values with computed deflections and forces from the original bridge configuration model gave the indication that the cable pre-strain of 2,25‰ is suitable for describing the initial cable stresses and will be used for analysis of the current bridge configuration. The deflections and forces, given in Table 3-8 below are resulting from self-weight including non-structural elements and are taken at middle of the span. The left side of Figure 3-15 showing the sidewalk is denoted as the upstream cable plane.

The reaction forces resulting from the weight of the main span and full length of cables are 7003 kN giving an evenly distributed loading over the main span of 83,4 kN/m. This is a 49% increase from the loading of the original configuration, mostly resulting from the heavier concrete deck.

Table 3-8: Deflections and forces in cable planes

Cable plane	Deflection δ [mm]	Main cable F [kN]	Suspenders F [kN]	Top chord F [kN]	Bottom chord F [kN]
Upstream	8,0	3519	160	22	-53
Downstream	19,0	3377	153	19	-91

*Deflection measured in stiffening truss bottom chord

The very small deflection values shown in Table 3-8 are quite coherent with the suspected horizontal layout of the bridge deck. Comparing with the +147 mm hogging of the original deck construction, presented in Table 3-5, the bridge has suffered a significant deformation of 139 mm in the upstream cable plane. Whether these deformations are of mainly elastic or plastic nature, or resulting from self-compaction or corrosion of the locked coil strands, is difficult to predict. Furthermore, this results in an increase in tensile forces of 37% and 40% in the upstream main cable and suspenders respectively. The maximum cable force occurring at the top of the west backstay where the vertical force component is at its highest value has now increased from 3057 kN, computed with the original configuration model, to 4188 kN (321 MPa). This is an addition of about 37% which is of potential concern with regard to the main cable factor of safety.

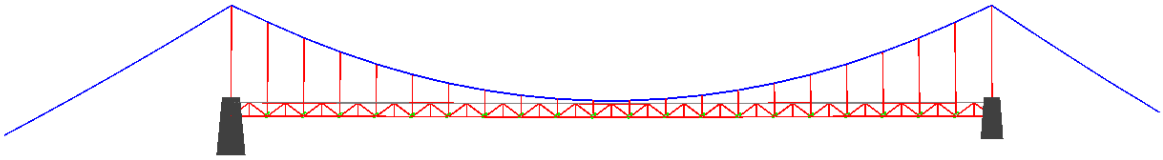

Figure 3-16: Deflected shape under dead load conditions (scaled)

The forces in the top and bottom chord are rather small due to the very little deflection experienced by the stiffening girder but will increase under traffic load in the form of pressure in the top chord and tension in the bottom chord. Table 3-5 gives an indication of the behavior of the top and bottom chords under different deflections, showing high tensile forces in the bottom chord under large deflections.

The locked coil strand cables comprising the main cable system of the bridge were evaluated by visual inspection in 2011. The cables were considered to be subjected to possible degradation due to corrosion making it an interesting case to analyze the effect of decreased cross section on deflections and forces, shown in Table 3-9.

Table 3-9: Decreased cable section in upstream cable plane

Cable cross section	Deflection δ [mm]	Main cable F [kN]	Suspenders F [kN]
100%	8	3519	160
95%	-11	3457	158
90%	-32	3405	156
85%	-55	3349	154
80%	-79	3290	152
75%	-106	3225	149
70%	-136	3155	147

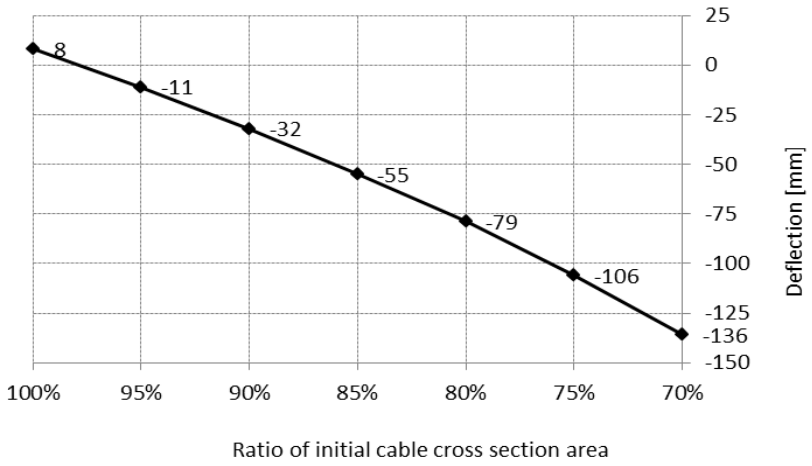

Figure 3-17: Deflections as function of degrading cable section

Table 3-9 and Figure 3-17 show the nearly linear descending trend of the computed deflection at mid-span when the main cable cross section area is decreased from being fully active to only 70%. The possibility of a whole 30% of the section area corroding away is a rather unrealistic case but in the case of a few percent loss of cable which is a likely scenario, it is important to consider effects on individual structural elements. The decrease in main cable force as the bridge deck deflects more extensively, shown in column three of Table 3-9, implies that an extended portion of the main span loading is being transferred from the cable system to the stiffening truss girder. It should be noted however that the loss in cable section is simulated over the full length of the cable. The deflections in Figure 3-17 may therefore be somewhat overestimated due to the fact that local loss of cable section, which is a more likely scenario, is unlikely to reduce cable forces throughout the full length of the cable. The reduced forces in the vicinity of the section loss will be regained to some degree in other parts of the cable by the action of friction forces between individual wires.

Following the discussion in the preceding paragraph; apart from the cables themselves degrading away, elements such as the top and bottom chords of the stiffening trusses will suffer a severe increase of compressive and tensile forces respectively when these increased deflections are added to traffic induced deflections. The design of the bridge by the Dorman Long Company (1945), based on the original weight of the bridge was carried out according to British Standard No 153 taking into account the self-weight of the structure and live load in the form of vehicle load with a 25% added impact loading. The documents show that the capacity of the I-section chords is nearly reached in the original design and with regard to the main span load increasing from 56,2 kN/m to 83,4 kN/m, the structural integrity of these members may be of some concern if large deformations occur.

Modal analysis

The following dynamic analysis of the current structural configuration of the bridge is conducted mainly under the same assumptions as for the dynamic analysis of the original bridge. A modal load case, using the stiffness resulting from the static nonlinear P-delta, large displacement load case as initial conditions, is analyzed for interpretation of mode shapes. The main difference is of course the considerably larger self-weight of the

superstructure and also a different modulus of elasticity. The assumed correct elastic modulus of 135 GPa is used instead of the 190 GPa used for modal comparison in the previous subsection.

Table 3-10: Modal analysis results

Model results		Participating mass ratio				
Mode nr	**Period, T [s]**	**U_X[1]**	**U_Y[1]**	**U_Z[1]**	**Shape[2]**	
1	1,137	1,1%	0,0%	77,0%	Vertical	S
2	0,706	0,0%	76,0%	0,0%	Transverse	S
3	0,676	5,1%	0,1%	0,0%	Vertical	A
4	0,475	0,0%	5,2%	0,0%	Torsion	-
5	0,428	0,0%	0,0%	0,0%	Cables	-
6	0,421	0,0%	0,0%	0,0%	Cables	-
7	0,399	0,0%	0,0%	0,0%	Cables	-
8	0,392	0,0%	0,0%	0,0%	Cables	-
9	0,380	56,0%	0,0%	1,7%	Vertical	A
10	0,327	0,0%	0,1%	0,0%	Torsion	-
15	0,298	30,0%	0,0%	8,3%	Vertical	A
18	0,240	0,0%	0,4%	0,0%	Transverse	S
24	0,208	0,0%	0,5%	0,0%	Torsion	-
29	0,202	1,3%	0,0%	0,0%	Vertical	A
54	0,146	0,6%	0,0%	3,5%	Vertical	A
73	0,117	0,0%	4,7%	0,0%	Torsion	-
74	0,116	0,0%	8,3%	0,0%	Torsion	-

[1)] x-axis is longitudinal, y-axis transverse and z-axis vertical
[2)] S=symmetric, A=Asymmetric.

Table 3-10 shows the natural periods and participating mass ratios of the ten first mode shapes and seven further shapes influencing the total mass translation of the structure. The first two shapes, vertical symmetric and transverse symmetric, contribute a large portion of the mass movement in the vertical and transverse directions while asymmetric vertical shapes contribute to longitudinal movement of the structure. Although comparison between mode shapes of the two models is not quite accurate due to different stiffness of the cables, it may be noted by also looking at the model results of Table 3-7 that the first three shapes are of the same form, yielding very similar mass participation ratios. The main difference lies in the mass difference of the two models enforcing a longer natural period of the first mode shape of the heavier current bridge construction. Figure 3-18 to Figure 3-23 show the most relevant modal shapes of the bridge scaled 2000/1.

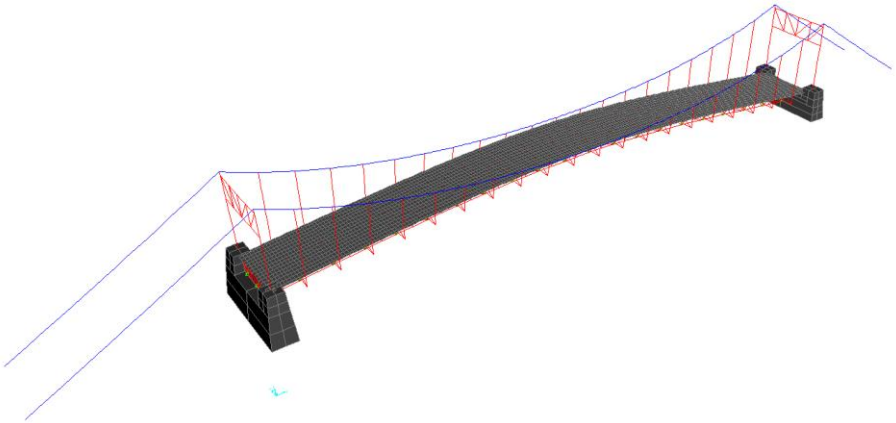

Figure 3-18: Mode 1, T=1,137s - 1st vertical mode, (current bridge configuration)

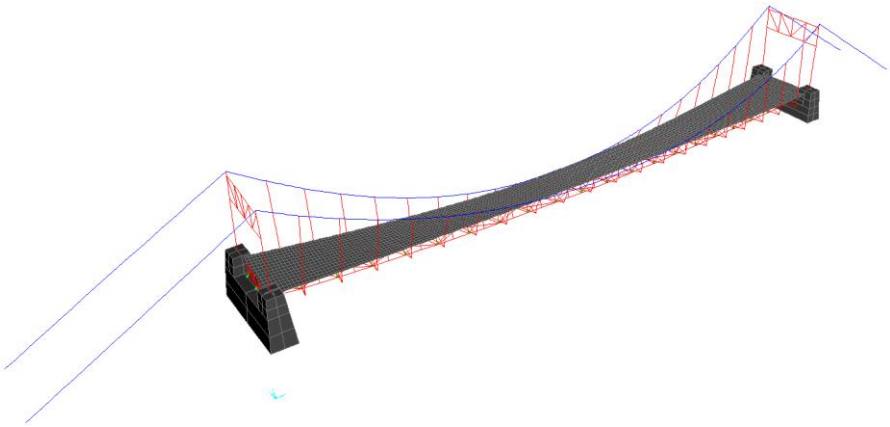

Figure 3-19: Mode 2, T=0,706s - 1st transverse mode, (current bridge configuration)

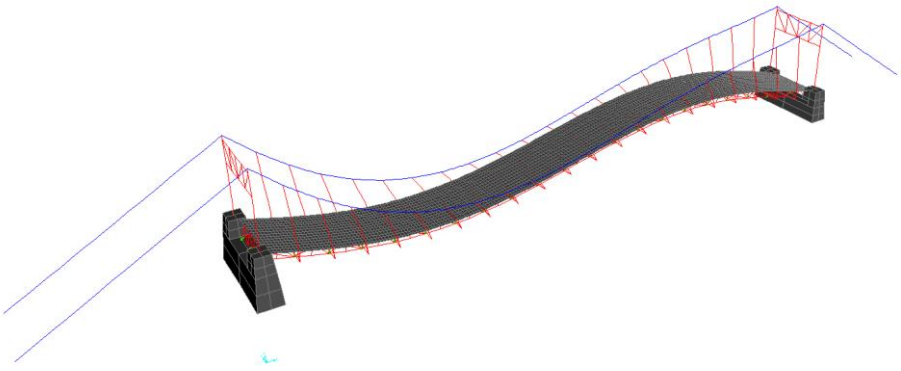

Figure 3-20: Mode 3, T=0,676s - 2nd vertical mode, (current bridge configuration)

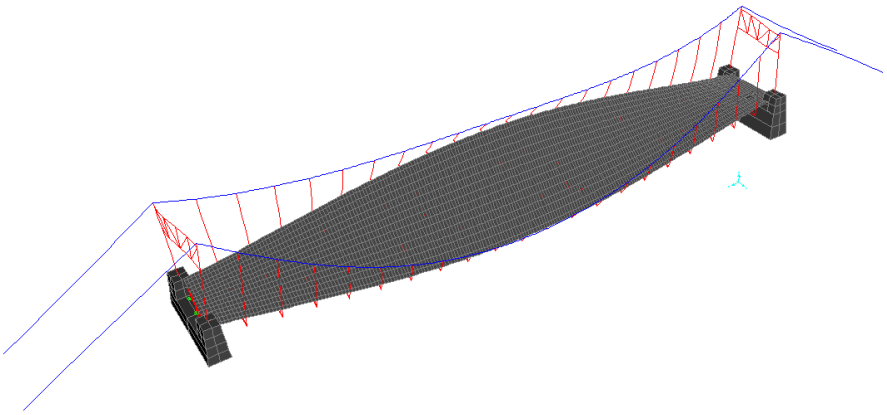

Figure 3-21: Mode 4, T=0,475s - 1st torsional mode, (current bridge configuration)

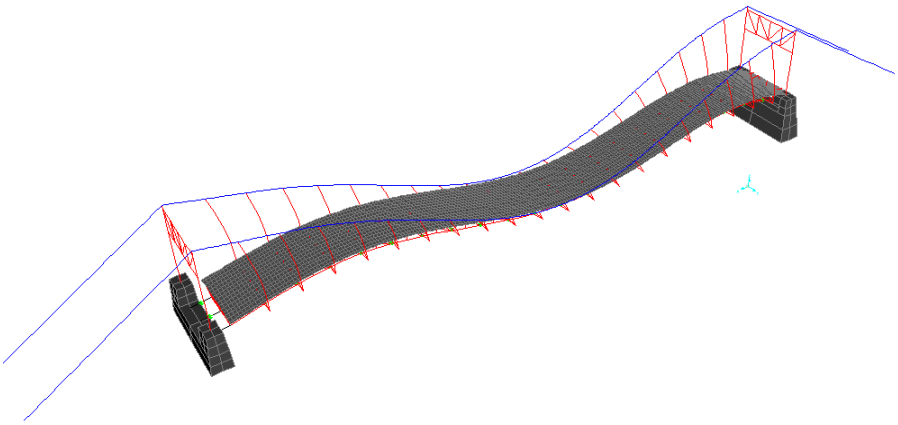

Figure 3-22: Mode 9, T=0,380s - 3rd vertical mode, (current bridge configuration)

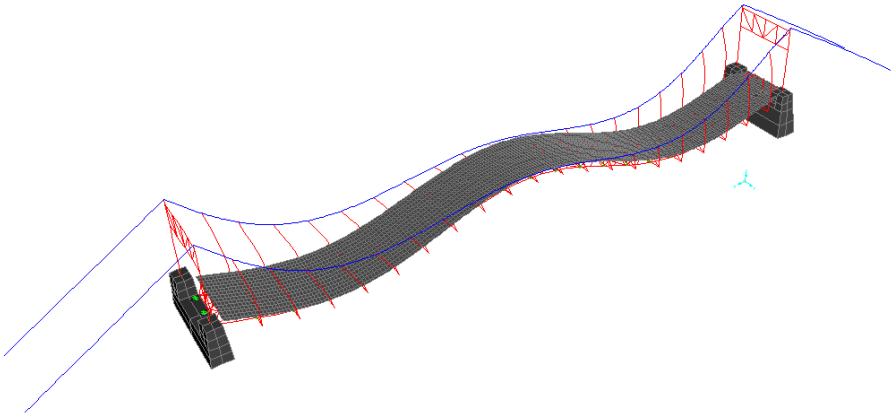

Figure 3-23: Mode 15, T=0,298s - 4th vertical mode, (current bridge configuration)

The modes chosen for display are the ones considered as the most interesting in terms of natural periods and mass participation according to Table 3-10. With relation to the scheduled vibration tests on the bridge, suitable placements of accelerometers to capture the movements of the significant modes may be estimated by studying Table 3-10 and the above figures. Figure 3-18 and Figure 3-19 show the first two mode shapes where accelerometers placed at the up- and downstream side of the main span centerline should capture the largest deflections of the deck. The third mode given in Figure 3-20 expresses maximum movement of the bridge deck in the vicinity of the main span quarter points, and the deck movement in the torsional mode in Figure 3-21 indicates that triaxial accelerometers placed at the up- and downstream side of the main span centerline would capture the largest deflections imposed to the bridge. An example of a potential accelerometer set-up for vibration tests is given in Figure 3-29. Further presentation of vibration based methods is provided in subsections 4.1.1 through 4.1.3 of this thesis.

The summarized results in Table 3-10 express a tendency of the bridge to move in vertical translation instead of lateral. This domination of vertical, torsional and cable movement shapes may be concluded to be caused by the stiff concrete deck resisting lateral movement and also because the main span is only 84 m long. The required number of modes to reach an effective mass ratio of 90% is 79 in the longitudinal direction, and 75 and 300 in the transverse and vertical directions, respectively.

To conclude the dynamic analysis of the bridge model, the effect of main cable degradation on the natural periods of the first five mode shapes is studied.

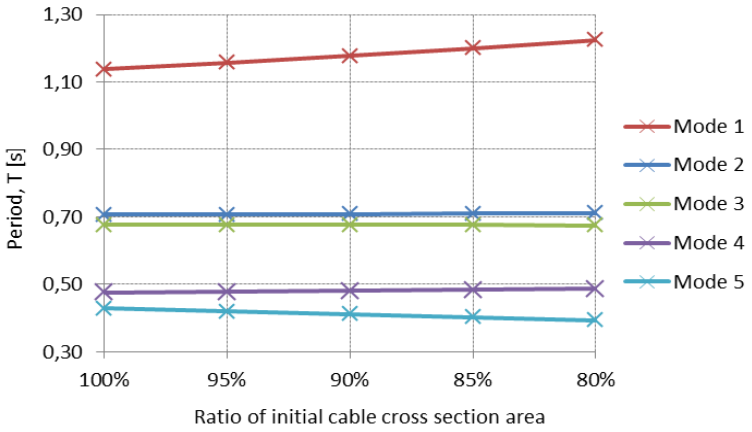

Figure 3-24: Natural periods as function of degrading cable section

Figure 3-24 shows slightly larger values of period length for the first mode as the cable cross section area is reduced. The next four modes inspected experience minimal deviation from the initial values of the full cross section.

Traffic loading

In addition to the self-weight of the suspension bridge, moving vehicular traffic is a concern regarding structural performance. The heaviest vehicle considered in the design of the original bridge configuration in 1945 was a 16 ton truck with an additive 25% impact load, a total of 20 tons. Today, trucks weighing significantly more are common which

implies for the need to perform some sort of analysis on the induced effects from such loading.

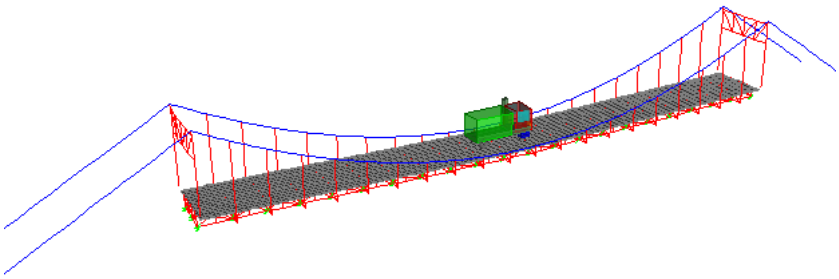

Figure 3-25: Truck load simulation

The following traffic load analysis is performed by defining a load combination comprising the dead load of the structure and a vehicle load case using the software CSI Bridge v15. Two types of vehicle load cases are defined where the stiffness at the end of the static nonlinear P-delta, large displacement case is utilized for initial conditions. The first case to be analyzed involves several trucks, weighing from 200 kN to 1000 kN driving across the bridge. This form of analysis is intended to prove as beneficial in terms of comparison with measurements of vehicle induced deformation from planned tests. A successfully validated model will then provide information about structural response such as the severity of stresses and deformations resulting from traffic loading. The latter moving load case to be investigated involves a design load combination of load model 1 according to Eurocode 1, Traffic loads on bridges (CEN, 2003b). Load model 1 involves vehicle and evenly distributed loading acting on 3 m wide notional lanes which are defined according to the width between curbs of the considered bridge. In the case of the 6,2 m wide Ölfusá Bridge, two notional lanes are defined; lane 1, illustrated by blue color in Figure 3-26, carries a 600 kN vehicle and evenly distributed loading of 9 kN/m^2 while lane 2 (red) carries a 400 kN vehicle and loading of 2,5 kN/m^2. Lane 1 is on the downstream side of the bridge deck while lane 2 runs beside the sidewalk on the upstream side. Results of a design load combination involving load model 1 are given in Table 3-12.

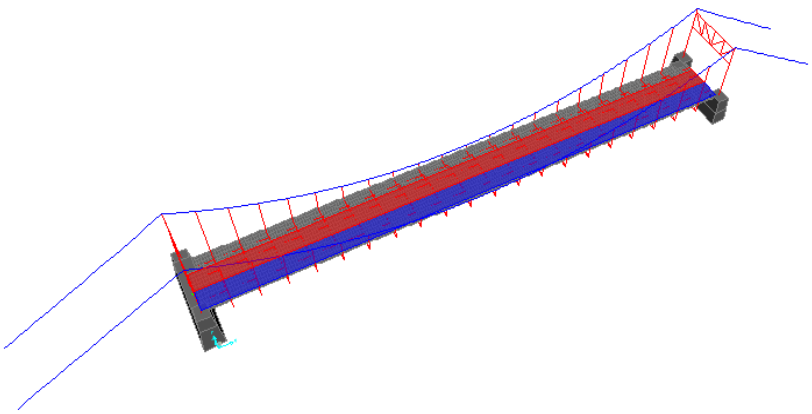

Figure 3-26: Lane definition for load model 1

Table 3-11 presents deflection- and cable force values of the truck loading analysis. An un-factored characteristic load combination including self-weight of the structure and a single truck weighing 200-1000 kN is defined and a multi-step static analysis is carried out. This type of analysis calculates a separate linear static solution for each time step that is defined while the truck drives over the bridge (Computers and Structures, 2011) providing a basis for comparison with potential static vehicle measurements. Figure 3-27 and Figure 3-28 illustrate the trend in vehicle induced deflections and cable forces in relation to values resulting only from the self-weight of the structure.

Table 3-11: Truck loading results

Truck weight	Upstream deflection	Downstream deflection	Upstream cable force	Downstream cable force	Maximum cable force at tower
[kN]	δ [mm]	δ [mm]	F [kN]	F [kN]	F [kN]
200	-9,0	20	3605	3527	4290
300	-18	20	3648	3603	4340
400	-26	-29	3690	3678	4391
500	-34	-41	3733	3754	4466
600	-43	-54	3776	3829	4555
700	-51	-66	3819	3904	4645
800	-60	-78	3862	3979	4735
900	-68	-90	3904	4055	4824
1000	-76,0	-103	3947	4130	4914

*Deflection measured in stiffening truss bottom chord

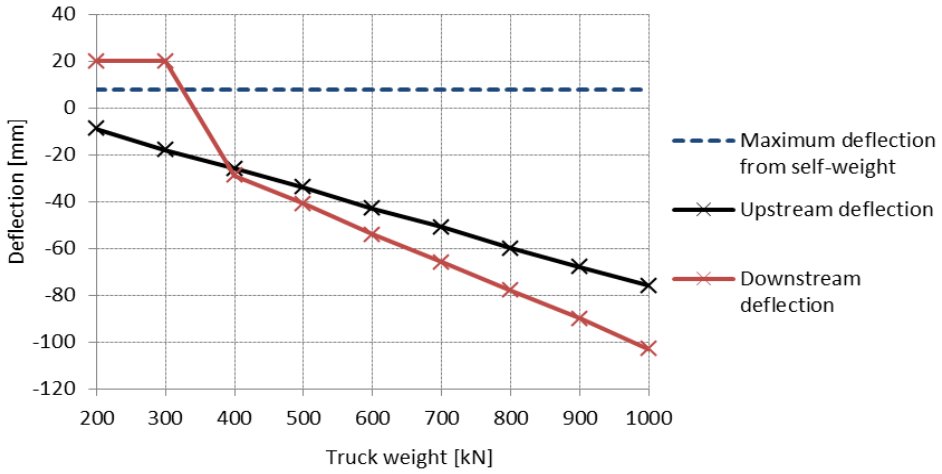

Figure 3-27: Truck loading: Mid-span deflections

The deflection values plotted in Figure 3-27 describe the transverse behavior of the bridge deck at the middle of the 84 m long main span. As before, the heavier side of the deck including the sidewalk is denoted as the upstream side while the downstream side is considerably lighter. The uneven weight distribution affects the computed deflections of Figure 3-27 where the weight of the lightest trucks, travelling in the downstream lane 1, does not fully counteract the large self-weight of the upstream part of the deck. As the weight of the trucks increases however, the downstream side of the deck deflects considerably more. The reason for choosing lane 1 for truck simulation (blue lane in Figure

3-26) is that it is located at a larger eccentricity from the middle longitudinal axis of the bridge than lane 2, thus providing the most severe values of deflections and forces induced from the heavier vehicles.

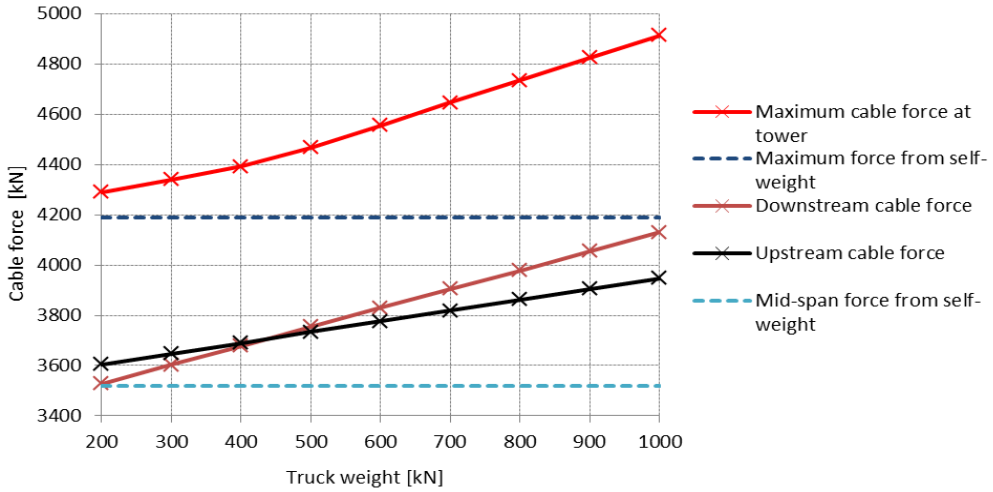

Figure 3-28: Truck loading: Main cable forces

The downstream and upstream main cable forces plotted in Figure 3-28 are quite consistent with the deflection values in Figure 3-27: The lightest vehicles (200-400 kN) induce smaller forces in the downstream cable plane where the deflections are smaller while the heavier vehicles (over 400 kN) induce larger forces in that plane accompanied by larger deflections in Figure 3-27. The figure also shows a significant increase of the maximum cable force at the bridge tower (red line) when the traffic loading is added to the self-weight which is given with the dashed dark blue line.

The main objective of analyzing the effects of a design load combination including load model 1 is to provide an evaluation of the main cable strength criteria according to modern design standards. The following combination describing the loading at the ultimate limit state of the structure yields the results in Table 3-12.

$$\gamma_G G_k + \gamma_{Q,1}\left(\alpha_Q Q_{ik} + \alpha_q q_{ik}\right) \qquad [3.26]$$

The partial safety factors, γ_G for the self-weight and $\gamma_{Q,1}$ for the imposed loading of load model 1, are both taken as 1,35. Q_{ik} and q_{ik} are the previously described characteristic vehicle- and evenly distributed loads acting in lanes 1 and 2, respectively. The reduction factor for bridge loading is taken as α=1.

Table 3-12: Load model 1 results

Cable plane	**Deflection**	**Main cable**	**Suspenders**	**Max. cable force at tower**
	δ [mm]	**F [kN]**	**F [kN]**	**[kN]**
Upstream	-319,0	6646	313	7901
Downstream	-388,0	7323	351	8711

*Deflection measured in stiffening truss bottom chord

The deflections, horizontal main cable forces and suspender forces in Table 3-12 are taken at the middle of the span where substantial deflections are noted in the downstream part of the bridge deck while the maximum cable forces of 8711 kN (667 MPa stress) occur in the backstay at the west tower. To put the critical downstream values of Table 3-12 in perspective, the design horizontal cable force, suspender force and maximum cable force were calculated in the original bridge design in 1945 as 3404 kN, 156 kN and 4037 kN, respectively.

By using the main cable strength given in subsection 3.2.2 as F_{Rk} = 15900 kN, the strength design criteria of F_{Ed} / F_{Rd} < 1,0 can be checked. The cable steel strength is reduced according to design standards (CEN, 2005) by a material factor of 1,5 which gives the following check:

$$\frac{F_{Ed}}{F_{Rd}} = \frac{8711kN}{15900kN / 1,5} = 0,82 < 1,0$$

The main cable factor of safety can be estimated by calculating an un-factored combination involving the same loads as before (load combination [3.26] above without partial factors). The maximum characteristic cable force at the west tower resulting from that combination is F_{Ek} = 6453 kN (which gives a stress of 494 MPa), yielding the following factor of safety:

$$\frac{F_{Rk}}{F_{Ek}} = \frac{15900kN}{6453kN} = 2,4$$

This is a rather low factor of safety whereas a factor of four is commonly employed in design and a factor of less than two is considered unacceptable. These calculations account for the uneven force distribution between the upstream- and downstream cable planes while they do not however include potential deterioration of the cable strength, thus accounting for full initial bearing capacity.

3.5 Main uncertainties of the modeling process

Table 3-13 summarizes the self-weight of the structural and non-structural elements that comprise the main span of the Ölfusá Suspension Bridge. The design load values given in the table are retrieved from the original design documents by the Dorman Long Company (1945). The main uncertainty regarding geometrical interpretation of the original bridge construction occurs in the modeling of the concrete deck. When the weight of the modeled deck (3100 kN in Table 3-13) of the original configuration is compared to the design weight (2786 kN), a deviation of about 10% is noted. The assumption is made that the design values are correct, and therefore the weight of the modeled concrete deck is scaled down to 2786 kN to match the design and provide a basis for comparison. The modeled steel construction including a 10% added weight to account for connections and rivets fits well with the design values as well as the weight of non-structural elements.

Table 3-13: Self-weight loading of the main span of Ölfusá Bridge

	Design loads		**Original configuration**		**Present configuration**	
	[kN]	[kN/m]	[kN]	[kN/m]	[kN]	[kN/m]
Concrete deck	2786	33,2	2786 (3100)	33,2	5149	61,3
Asphalt layer on roadway	528	6,3	528	6,3	-	-
Steel construction	1334,1	15,9	1334	15,9	1334	15,9
Parapets	70	0,8	70	0,8	126	1,5
IPE-140, supporting gondola	-	-	-	-	25	0,3
Pipelines + supporting angles	-	-	-	-	375	4,5
Total	4718	56,2	1932	56,2	7009	83,4

The most important aspect of the geometry of the present bridge configuration lies in the modeling of the concrete deck where the largest addition of weight can be noted. The present bridge deck is modeled quite accurately according to design drawings from 1992 revealing a self-weight increase of the deck itself going from 33,2 kN/m over the main span to 61,3 kN/m (see Table 3-13) which is about 85%.

A dominating factor regarding the structural performance of both models is the elastic modulus of the steel main cables. The assumed E = 135 GPa may potentially be of a lower value which would result in larger values of deflections and cable stresses while a higher modulus would induce the opposite effects. Other modeling uncertainties to be kept in mind may include the interpretation of boundary conditions, connection stiffness, cable geometry, and other geometrical readings from old design drawings.

In regard to potential calibration of the model with vibration tests, the parameters selected for updating are critical to enable successful model updating and depend on the judgment of the engineer (Xu & Xia, 2012). In this case, the parameters that are likely to be the most important in an updating process include the mass densities of the concrete deck and steel stiffening truss and the elastic modululus of the main cables.

3.6 Summary and accelerometer positioning

This chapter has presented a finite element model of the Ölfusá Suspension Bridge constructed for condition evaluation purposes and as basis for potential calibration with near future vibration measurements. Two separate models built on the same foundation were introduced; one comprising the original bridge deck and another one where the newer and significantly heavier deck installed in 1992 was modeled. A relatively thorough description of the actual bridge and modeling process was provided where section and material properties of structural elements are listed. Modeling techniques regarding all major structural components were discussed along with an overview of non-structural parts of the bridge. A section on theoretical methods related to the calculation procedures used by the applied software provides explanations regarding linear and nonlinear static analysis, fundamentals of dynamic analysis including aspects of both forced and free vibration, and finally a brief discussion on the finite element method.

Section 3.4.1, involving the original bridge configuration, included analysis of static and modal properties of the structure. The static part included an iterative procedure to find the correct degree of pre-strain to apply to the main cables to correctly model the hogged bridge deck under self-weight loading. This provided an initial state of the superstructure used for further analysis. The main objectives of this section were to validate the model by comparing reaction forces and cable forces to design values and by matching computed deflections to measurements from load tests conducted in 1946 and given in Table 3-6. It may be concluded that these objectives have been adequately fulfilled in terms of global level structural responses whereas deflection values of the first two of the performed load tests match with accuracy of about and less than 20% and the cable force at midspan is only about 9% off from design values. Deflections from the second two load tests, yielding values of only a few millimeters were however harder to interpret. The findings of the modal analysis where computed natural periods and previously reported values were compared, gave some indication of consistency although the difference in methods and assumptions is likely to have caused the considerable deviations shown in Table 3-7.

Section 3.4.2, where the present bridge configuration is analyzed, includes static, modal, and traffic analysis. The objectives of this section were to evaluate the effects of the heavier, unsymmetrical bridge deck and estimate the effects of cable cross section loss, to provide the natural periods of significant modes, and investigate vehicle induced effects. The static analysis indicated that the weight increase following the newer bridge deck had caused the deck to deflect from a hogging state of +147 mm at midspan to +8 mm and +19 mm in the upstream and downstream cable planes, respectively. The reaction forces showed an increase of about 49% in self-weight of the main span and at the middle of the 84 m long span, the upstream main cable and suspenders were shown to experience an increase in tensile forces of 37% and 40% respectively. Figure 3-17 gives an indication on how potential loss of cross section due to corrosion may affect structural behavior in terms of increased deflections of the bridge deck. The traffic analysis was conducted in two main steps: The first brought light on the structural performance of the bridge under vehicle loading where stepped loading of trucks weighing 200-1000 kN was simulated to act in union with the self-weight of the structure. The latter step involved a load combination including load model 1 according to Eurocode 1 – Part 2: Traffic loads on bridges (CEN, 2003b) where the main cable factor of safety was estimated as the rather low value of 2,4.

The natural periods which are summarized in Table 3-10 may be used as basis for calibration of the model with vibration tests where computed frequencies are correlated with corresponding measurements. These results of the modal analysis are furthermore intended to assist in the positioning of accelerometers for the vibration tests. Figure 3-18 to Figure 3-23 in the modal analysis part of subsection 3.4.2 showing mass contributing mode shapes are discussed with regard to practical positioning of accelerometers, intended to capture movements of the first shapes. The discussions provided from the modal analysis of the current structural configuration have led to the example presented in Figure 3-29:

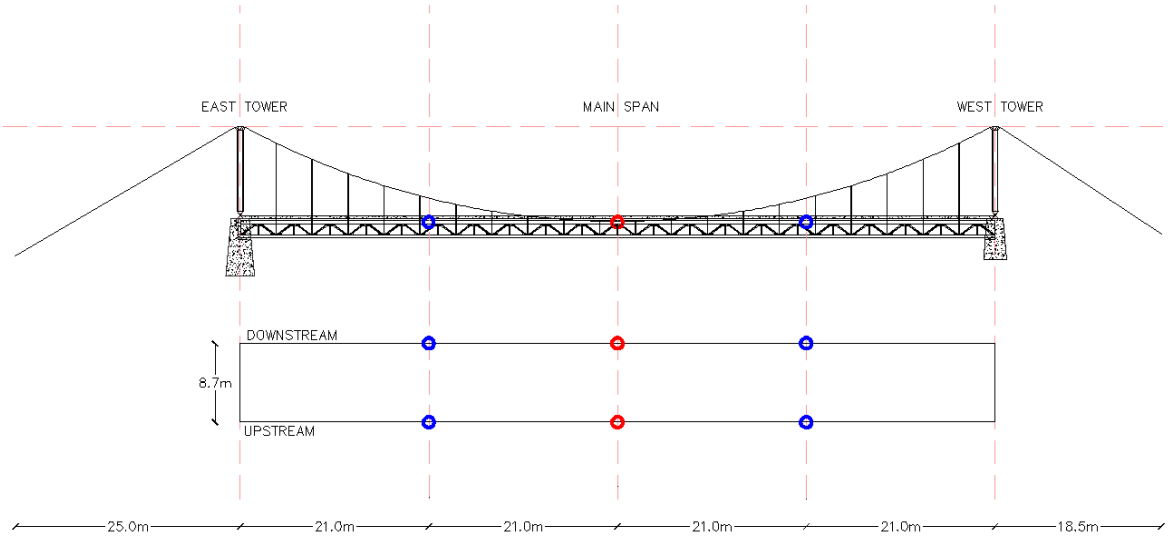

Figure 3-29: Potential positioning of accelerometers

Figure 3-29 gives an illustrative example of accelerometer positioning involving four uniaxial and two triaxial devices following the preceding discussions. The blue marks in the figure indicate the uniaxial accelerometers and the red marks indicate triaxial ones. On forehand, mid- and quarter span placements of accelerometers may have been somewhat expected as suitable for capturing modal shapes but nonetheless it is important to provide a fairly reliable verification on any assumptions made in advance.

4 Damage detection and structural health monitoring

The main objective of this chapter is to provide an overview of available structural damage detection and health monitoring methods, and discuss potential application of these methods for short span bridges such as the Ölfusá Suspension Bridge. The selection of topics is conducted with regard of the system configuration and structural condition of the Ölfusá Suspension Bridge to give a broad perspective on which measures may be appropriate in terms of evaluation and structural life estimation of the bridge.

The first sections of the chapter address structural damage detection in the form of vibration- and non-destructive methods, and also a discussion on cable corrosion and cable force estimation is provided. Damage detection techniques in the form of visual inspection are not discussed in detail whereas the bridge has recently undergone such an inspection. Later sections of the chapter present aspects of structural health monitoring of bridges with the main focus on general objectives of monitoring and description of potential measurement scenarios.

It is attempted to maintain the discussion on monitoring systems in perspective with potential applicability to the Ölfusá Bridge although most references to complete systems tend to relate to longer span suspension bridges.

4.1 Structural damage detection

The exposure of civil structures to loading in the form of natural hazards such as harsh weather conditions and earthquakes, and man-made hazards such as fire and collisions may lead to excessive damage of structural elements and even collapse. In union with possible structural defects and increase in applied traffic loading, this exposure to the environment makes suspension bridges, in particular the ones of high age vulnerable to structural damage, often in the form of corrosion and long term fatigue. In order to detect progressive damage of bearing elements, different methods may be implemented for early identification enabling maintenance or traffic regulations before a potential collapse of the structure. Global methods focusing on the complete structural system are commonly employed for examining the global properties of the structure while methods considering structural elements at a local level are used to determine the more exact nature of the damage. Damage detection methods utilizing the vibrations properties of the structure are regarded as global methods and non-destructive testing as local approaches (Xu & Xia, 2012).

The concept of damage identification is well described by a classification system defining four levels of the process, introduced by Rytter (1993):

- Level 1: Determination that damage is present in the structure
- Level 2: Determination of the geometric location of the damage
- Level 3: Quantification of the severity of the damage
- Level 4: Prediction of the remaining service life of the structure

The majority of damage detection methods are limited to level 1 to level 3. Level 4 methods, predicting the remaining service life of the structure requires interdisciplinary coupling of fracture mechanics, fatigue life analysis and structural reliability and are still rather limited in application (Doebling et al., 1998; Xu & Xia, 2012).

Vibration based damage detection makes use of vibration properties of the structure which are measured in field tests or by using different types of monitoring equipment. The properties, in the form of for example response time histories and global vibration characteristics are functions of the physical properties of the structure such as the mass, stiffness, damping and boundary conditions (Xu & Xia, 2012). Changes in the vibration properties indicate alteration in the physical structural properties as result of possible damage. The linkage between the vibrational and physical characteristics provides a relatively confident basis for identification of damage and can also be used for evaluation of tension force of stay cables. The effects of the damage may be classified as linear or nonlinear, linear being defined as when the initially linear-elastic structure remains linear-elastic after damage. Nonlinear damage can then be defined as the case when the initially linear-elastic structure acts in a nonlinear manner after the introduction of damage. Loose connections and formation of fatigue cracks are examples of damage that exhibit nonlinear behavior to the structure after formation. The majority of damage detection methods address only the problem of linear damage detection (Doebling et al., 1998). For linear methods, a differentiation is made between non-model based methods which compare dynamic parameter changes before and after the occurrence of damage, and model-based methods which involve iterative adjustment of structural parameters. Vibration based methods applied without structural model calibration primarily provide level 1 and level 2 damage identification while the coupling with a structural model does in some cases enable level 3 damage identification (Doebling et al., 1998).

The category of vibration based damage detection techniques includes the analysis of frequency changes, mode shape changes, modal damping changes, changes in the frequency response function matrix, mode shape curvature changes, modal strain energy changes and flexibility changes (Doebling et al., 1998; Xu & Xia, 2012). Non-destructive testing methods are applied to provide an evaluation of the structural health and to detect material changes, often at a more local level compared to vibration methods. Various methods have been developed in this sense for different fields including damage detection in civil structures such as suspension bridges. The commonly employed techniques suitable for civil structures include the magnetostrictive method, acoustic emission method, ultrasonic pulse velocity method, impact-echo method, radiography method and eddy current method.

The following subsections provide brief descriptions of the vibration based and non-destructive damage detection methods which may be considered to be relevant for short span suspension bridges such as the Ölfusá Bridge.

4.1.1 Frequency Changes

Measurement of frequency shifts has been a widely used structural damage detection method because the natural frequency is the most fundamental vibration parameter (Xu & Xia, 2012). The observation that changes in the structural system, such as extensive deformations or the failure of local elements may alter the vibration frequencies has stimulated the development of modal methods for damage identification and health monitoring. These modifications of the vibration modes yielding changes in natural frequencies, mode shapes and modal damping values can be obtained from results of dynamic testing (Salawu, 1997).

The method of interpreting changes in frequency may either be conducted using mathematical models including known structural damage as comparison with measured frequencies for identification or by direct determination of damage parameters from the frequency shifts (Doebling et al., 1998). The former, categorized as level 1 damage detection, is outlined with an example given by Cawley and Adams (1979) starting with the ratio between frequency shifts for two different natural modes. A grid of potential damage points is presented and the measured frequency shifts are related to the model predicted ones using an error term based on a local stiffness reduction. A number of mode pairs are considered for each location on the grid and the pair yielding the lowest error indicates the location of the damage. The latter is typically classified as a level 2 or level 3 damage identification method (Doebling et al., 1998).

The nature, location and severity of evident damage affect the modal parameters in a way that changes may not be the same for each mode, offering possible usage of dynamic test results for detection, location and quantification of damage. Acquisition of responses is performed using some form of transducer which monitors the structural response to either artificially induced excitation or ambient forces under regular service conditions. In the case of detected changes in the natural frequencies, potential damage or deterioration of the structure may be assumed. Descending frequencies tend to infer reduction in stiffness while frequencies higher than expected are indicative of supports stiffer than expected. A confidence level of about 5 percent is considered as an adequate indicator of significant change in frequency although care must be taken due to ambient conditions like temperatures changes which may cause even greater changes within a single day. Determination of the location of potential damage has been widely reported yielding relatively uncertain documented results. Structural defects are considered likely to be detected in the vicinity of modal nodes which are points of zero modal displacements where the stress is minimal for the particular mode of vibration. The distinction of damage in regions of low stresses is however assumed to be rather unreliable indicating that alteration in natural frequencies alone might not provide sufficient confirmation of detected damage unless the damage occurs in an important load bearing member. Adding to this discussion, some experimental and numerical studies have indicated that lower modes of vibration are best suited for general damage detection while others have pointed out an increased sensitivity of the higher modes to local damage (Salawu, 1997).

Estimation of the tension in stay cables of cable-stayed bridges can be obtained by measurement of natural frequency. Loss in cable tension may be concluded if the estimated frequency values are significantly lower than design values. Potential breaking of wires or deterioration must though be kept in mind due to resulting reduction in cross section which reduces strength but may not alter tension forces (Salawu, 1997). Cable force estimation is addressed in section 4.3.

To obtain accurate results from frequency tests, either very exact measurements must be obtained or significant damages must be present due to the somewhat low sensitivity of frequency shifts to damage in structural systems. Also, a more progressive analysis than identification of level 1 is difficult to obtain due to the modal properties being a global characteristic of the structure although higher modal frequencies, if available, may provide a necessary association with local responses to locate damages (Doebling et al., 1998).

Despite uncertainties regarding exact placing of damaged members, the application of damage detection in the form of frequency change analysis is advantageous in the sense that precise measurements can be conducted using very few sensors. The measurements are of low cost and compared to other parameters, the values of natural frequencies may be obtained with high accuracy. The values can then be applied for further analysis including model updating and verification of analytical models describing actual civil structures such as suspension bridges. This type of procedure will be conducted subsequent to the scheduled vibration tests of the Ölfusá Bridge.

4.1.2 Mode shape changes

The analysis of mode shape changes for damage identification or structural health validation generally makes use of the modal assurance criterion (MAC) or the coordinate modal assurance criterion (COMAC). The MAC value gives an indication of correlation between two sets of mode shapes and COMAC which relates to the degrees of freedom of the structure indicates the correlation between the mode shapes at a selected point of measurement on the structure (Williams & Salawu, 1995). The use of MAC and/or COMAC is applicable for both the identification of correlated mode pairs of structural models and experiments, and also mode pairs before and after damage if measurements are available.

Considering the correlation between two sets of measurements representing the structure, the MAC is defined by Allemang and Brown (1983) as:

$$MAC\left(\{\phi_A\}_q, \{\phi_B\}_r\right) = \frac{\left|\{\phi_A\}_q^T \{\phi_B\}_r\right|^2}{\left(\{\phi_A\}_q^T \{\phi_A\}_q\right)\left(\{\phi_B\}_r^T \{\phi_B\}_r\right)} \qquad [4.1]$$

Where $\{\phi_A\}_q$ and $\{\phi_B\}_r$ are mode shape vectors for modes q and r of data sets A and B, respectively. A MAC value close to 1 indicates significant correlation of the two modes whereas a value close to 0 is indicative of uncorrelated modes (Williams & Salawu, 1995). COMAC values may be computed in a relatively similar manner for datasets A and B for measurement at a certain location in a system:

$$COMAC(i) = \frac{\left(\sum_{i=1}^{L}\left(\phi_A{}^{i}\right)_l\left(\phi_B{}^{i}\right)_l\right)^2}{\left(\sum_{i=1}^{L}\left(\phi_A{}^{i}\right)_l{}^{2}\right)\left(\sum_{i=1}^{L}\left(\phi_B{}^{i}\right)_l{}^{2}\right)} \quad [4.2]$$

The correlated modes from the datasets are paired; here with *i* denoted as the measurement location. $(\phi_A{}^{i})_l$ is an element of mode shape vector for set *A* in correlated mode pair *l* with *L* being the total sum of correlated mode pairs. A COMAC value close to 1 indicates good correlation of the two datasets at the selected node of the structure.

Due to different energy distribution from each mode of vibration, any localized damage will affect each mode in a different manner depending on the location and severity of the damage. This has been investigated confirming that the COMAC is capable of locating structural damage to some degree of accuracy (Williams & Salawu, 1995; Xu & Xia, 2012). With regard to the application of modal shape methods, it is considered difficult to obtain high quality data from full-scale on-site tests. Resulting from full scale dynamic tests on a reinforced concrete bridge, Williams and Salawu (1995) suggested a MAC threshold value of 0,8 and at least 5% change in frequency as adequate indication of present damage. In practical applications, environmental conditions such as temperature and humidity are likely to affect the dynamic structural response and should be accounted for.

Summarizing the applicability of these methods, the MAC matrix may be used as an indicator of whether damage is present in the structure while evaluation of COMAC values is intended to identify the location of any defect. The outcome of the procedure is dependent of whether or not the modes and measurement locations can properly reflect the damage. Following a successful identification of damage prone areas, nondestructive test methods can be used for detailed inspections (Williams & Salawu, 1995).

4.1.3 Other vibration-based methods

As mentioned earlier in this section there are numerous vibration based methods that have been developed for structural damage detection. The analysis of frequency and mode shape changes described in the subsections above are commonly used, and relevant for damage evaluation and model validation of suspension bridges. The following descriptions are summarized from Xu and Xia, (2012) to briefly present some of the alternative vibration-based methods available.

Modal damping changes

The method of modal damping changes is conducted by extracting structural modal damping ratios but is not considered to yield the same accuracy as frequency and mode shape extraction. The use of modal damping ratios for damage indication is therefore not a commonly employed method.

Mode shape curvature changes

Analysis of mode shape curvature changes is an alternative to using the mode shapes directly and is based on the decreasing flexural stiffness causing an increase in curvature.

Being a derivative of the mode shapes, the calculation of the curvatures is error sensitive because a small noise in the mode shapes is likely to cause significant alterations in results.

Modal strain energy changes

The method using the derived modal strain energy changes as the damage indicating property is similar to the method of curvature changes, rather limited in application.

Changes in the frequency response function

Changes in the frequency response function have for example been used for detection of cracks in concrete girders and decks, yielding variable results but also for identification of damage in shear connectors in composite bridges providing more constant findings.

Flexibility changes

The method of flexibility changes encountered in the flexibility matrix has been tested by application to detect artificial cuts in a steel beam in the I-40 bridge over the Rio Grande in New Mexico yielding unsuccessful practical results.

4.1.4 Magnetostrictive technology

In the case of non-destructive damage detection, guided waves generated by magnetostrictive sensors can be used for effective inspection for discontinuities in civil structures including steel cables of suspension bridges. The high velocity waves which propagate along the element under inspection, guided by the geometric boundaries of the medium, are generated by the magnetostrictive effect of the sensor. This effect is initiated by an externally applied magnetic field which causes a small, but detectable physical alteration in the dimensions of ferromagnetic materials. Potential damage in a structural element may be detected by launching short pulses of waves which are then reflected by geometric irregularities in the form of discontinuities or welds. The time and amplitude of the received signal provide information on the location and degree of damage (Kwun et al., 2011). Magnetostrictive sensors have been under active development by the Southwest Research Institute in San Antonio, Texas since 1992. They were initially designed for evaluation of steel cables but have also been applied in operations such as pipeline inspection and onboard sensing of vehicle crash events for airbag design (Kwun & Bartels, 1998).

This method has been systemized for bridge cable inspection in the CableScan service, developed by the Canadian based company Pure Technologies. The service is reported to be capable of identifying structural anomalies such as corrosion and other defects in suspenders and bridge cables from a single location on each cable using lightweight equipment.

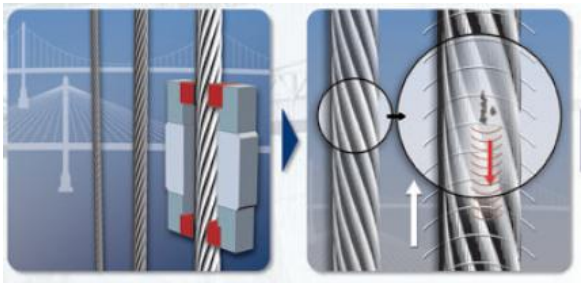

Figure 4-1: Generation of guided waves (Pure Technologies)

Figure 4-1 illustrates the initial steps of the CableScan service where guided waves generated by the magnetostrictive sensor propagate in axial direction along the cable. Defects and cross sectional changes then cause reflection of the waves which are detected by the sensor. The last step of the process, not shown in the figure involves a comprehensive analysis of the cable condition which may include an estimation of cross sectional loss along the free length of the cable and localization of damage. Furthermore, the condition of the cable is ranked which is beneficial in terms of comparison with other cables and future inspections (Pure Technologies). The magnetostrictive technology offers effectiveness and accuracy in terms of non-destructive damage detection because of its long inspection range and adequate sensitivity to defects (Kwun et al., 2011). The main drawbacks however should be regarded as difficulties in damage identification around cable clamps and tower saddles where connecting parts interfere with the wave signals.

4.1.5 Acoustic emission method

Although this method has mostly been applied for long-span suspension bridges with parallel wire strands comprising up to thousands of individual wires, it is applicable to most types of suspension and cable-stayed bridges in addition to pre- and post-tensioned bridges and will be discussed in some detail. Acoustic emission may be described as the occurrence of transient stress waves generated by rapid energy release resulting from cracking or some other source of disruption in a material. Severe loading conditions affecting bridge structures have been known to induce the formation of elastic waves due to damage mechanisms, especially in concrete and steel materials. The method of acoustic emission monitoring may be conceived as a non-invasive evaluation technique which enables continuous monitoring and has been the most widely used method for highway structural assessment (Nair & Cai, 2010).

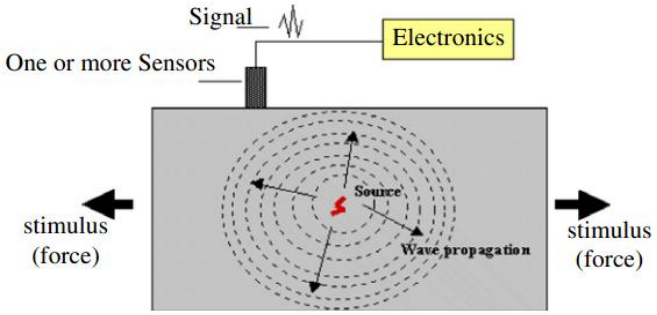

Figure 4-2: Principle of acoustic emission (Nair & Cai, 2010)

Figure 4-2 shows the components of the acoustic monitoring process. Deformation of the potentially damaged material induces a high frequency energy release that sensors detect as sound waves that propagate within the material. In addition to the generated acoustic emission waves and detection sensors as components of the process, understanding of the propagation characteristics of the waves is highly important for processing and interpretation of the collected data. The primary function of the sensors is to convert detected mechanical waves into electric signals which then are represented by characteristic parameters such as amplitude and duration. Typical sensors for acoustic emission monitoring are briefly described in section 4.4.3. The signals, visualized in Figure 4-3 may be interpreted using a certain threshold distinguishing unwanted emission from actual material deformation or breaking (Nair & Cai, 2010).

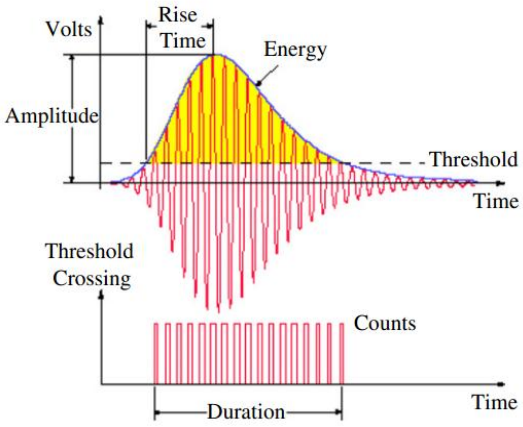

Figure 4-3: A typical acoustic emission signal (Nair & Cai, 2010)

In the case of suspension bridge application, the sensors are mounted on to the cables at discrete intervals to offer the best possible recognition of breaking wire signature analyzed by data acquisition software. The location of the wire break may then be estimated by analyzing the arrival time of the induced energy wave at different sensors. External ambient acoustic activity caused by factors such as loose bridge components and construction activity may interrupt and reduce the reliability in accurate detection of breaking wires and must be kept in mind in the otherwise effective process of locating wire breaks. The identification of damage prone areas will then allow for a more precise investigation of active corrosion and measurement of deterioration rate (Rankin et al., 2006). For distinction of emission originating from within the material of interest and

unwanted external emissions, acoustic emissions are generally classified into primary and secondary emissions.

Acoustic monitoring of bridge cables has been applied for over four decades. From successful experience with prestressed tendons, the technique was adapted for cable stay and suspension bridge cables leading to the conclusion that suitable detection and locating of wire breaks is well obtainable. The main advantages of using acoustic monitoring for bridge monitoring include the identifying of growing damage without disturbing highway traffic over the bridge. Reliability has increased with advances within source detection techniques and the method allows for live observation of disruption in materials due to advancements made in acquisition systems. Disadvantages include problems with background noise discrimination requiring qualified personnel for adequate installment and supervising. Furthermore, variable environmental and loading conditions for different types of bridges is prohibiting in providing standardized procedures for all bridge categories, emphasizing the need for specialized supervision (Nair & Cai, 2010).

In the case of structures subject to deterioration at an uncertain rate, levels of corrosion and fracture may be evaluated by using acoustic monitoring which may increase service life and avoid premature rebuilding by assuring adequate structural integrity (Barker & Tozser, 2011).

4.1.6 Other nondestructive test methods

In addition to the magnetostrictive method and acoustic emission monitoring outlined in the preceding subsection, there exist several nondestructive test methods which are applicable for damage detection in suspension bridges. The majority of these methods are however intended for damage detection in concrete elements and therefore not directly relevant for the main topic of this section, damage detection in cables. Some other methods involving wave propagation in cables do exist but are not as widely applied nor as developed as the previously described techniques. A short summary of methods is adopted from Xu and Xia, (2012), and Malhotra and Carino, (2004).

Ultrasonic pulse velocity

The ultrasonic pulse velocity method has been widely used for quality assessment of concrete. Strength, homogeneity, cement hardening, crack detection and deterioration of concrete may be estimated by connecting the velocity of compressive waves traveling through the material to elastic properties and density.

Impact echo

The impact echo method may be applied to detect flaws in concrete and is primarily used for testing piles but also concrete slabs. A high energy stress pulse is generated which propagates into the material and by measuring reflected waves, internal disruptions may be identified.

Infrared thermography

The infrared thermographic method has been recognized as an economical and accurate technique for assessment of pavement and bridge deck conditions. In the case of bridge

applications, temperature difference in solid materials is used to identify voids which cause disruption in conduction paths. An infrared camera is used to detect the difference in temperature on the material surface resulting from the disrupted thermal energy flow. The depth and thickness of the detected voids can though not be determined.

Radiography

Radiographic methods have been used for identification of defects in concrete, welded elements, castings and prestressing cables. Accurate information on internal characteristics may be obtained using radiography but the generally heavy equipment and large power consumption required tend to make the inspection process difficult in execution.

Eddy current

Eddy current testing provides flaw detection in conductive materials by using electromagnetic induction. Applications primarily include surface or subsurface crack detection but also estimation of corrosion in thin materials and the measuring of surface coating thickness. The method is favorable in the sense that very small cracks may be identified in the material surface vicinity and elements of irregular shapes can be inspected as long as the surface is accessible to the testing equipment. Defects occurring at some depth are however hard to detect because the eddy current density decreases with depth.

4.2 Steel cable corrosion

Corrosion in suspension bridge cables is stimulated by the presence of water and chemical solutions which tend to penetrate cable protective systems and cause damage to the steel cables. Environmental factors such as moisture, salt spray and the amount of pollutants and dissolved gases in the bridge atmosphere highly affect the rate of potential corrosion development (Mayrbaurl & Camo, 2004). Compared to other structural steel elements such as solid bars and rolled wide flange sections, cable bundles comprising a large number of thin wires are very susceptible to surface corrosion. Inaccessibility of internal wires makes inspection and maintenance problematic which allows for uninterrupted accumulation of cavities between wires (Gimsing, 1998). Due to this sensitivity to corrosion, various forms of cable protection systems are under constant development.

4.2.1 Corrosion effects and classification

Nakamura and Suzumura (2011) conducted extensive research on the deterioration of bridge cables and the effectiveness of different protection methods. The investigation included estimation of tensile and fatigue strength and elongation of corroded steel wires on three corrosion levels which were produced at laboratories. Specimens of galvanized and bare steel wires were subjected to aggressive conditions for different timeframes producing level one, two and three corrosion, defined by mass loss and appearance. Measurements revealed that both the galvanized and bare specimens experienced exponentially increasing loss of mass with elapsed time. Static testing showed that the tensile strength does not decrease according to level of corrosion for both galvanized and

bare steel specimens while decrease in elongation is detected as the steel part of the specimen starts to corrode. This causes serious problems in terms of material ductility due to the relation between elongation and ductility properties. Cyclic loading tests showed significant decrease in fatigue strength as the bare steel started corroding after the galvanized layer had corroded away.

The National Cooperative Highway Research Program, (Mayrbaurl & Camo, 2004) has published a report on inspection and strength evaluation of suspension bridge parallel wire cables where corrosion of galvanized wires is classified into four different stages:

- Stage 1 – spots of zinc oxidation on the wires
- Stage 2 – zinc oxidation on the entire wire surface
- Stage 3 – spots of brown rust covering up to 30% of the surface
- Stage 4 – brown rust covering more than 30% of the surface

4.2.2 Cable protective systems

Several methods have been proposed for cable protection, some outlined by Mayrbaurl and Camo (2004): Zinc coating of cable wires is a typical protection measure which may either last indefinitely or become depleted within 20 years, depending on the integrity of the exterior protective system. Grease and oil coating as wire protection has also been used for a long time providing excellent protection of the cables of for example the Brooklyn Bridge and the Manhattan Bridge. In some cases though, localized depletion has caused problems in terms of cracked or fully torn wires. Pastes such as red lead paste, zinc-based paste and lead and calcium-based paste have been applied as protection under wrapping wires of parallel wire cable systems. More recently zinc-based products have been preferred due to health concerns regarding the red lead paste. Combinations of wire wrapping and different paint systems have also been used. The most recent development in cable protection is the injecting of dehumidified air into the cable which is intended to keep the relative humidity inside the steel wire wrapping of the cable at or below 40% to provide a non-corrosive environment for the steel wires.

Nakamura and Suzumura´s research (2011) involved a comparison of prevention methods for parallel wire strands where seven repair methods were compared according to mass loss due to corrosion. The seven cases included:

- The use of no surface protection
- Epoxy resin paint on surface wires
- Zinc rich paint on surface wires
- Coating and filling the surface and inside wires with epoxy resin paint
- Filling the inside with oil

- Thick layer of zinc powders on surface layer
- Dehumidification.

Results showed that dehumidification of the wires was the most effective in slowing the progress of corrosion followed by the epoxy resin coating and filling, the zinc powder paste, the zinc and epoxy resin paint on only the surface wires and finally the oil filling.

Figure 4-4: Locked-coil strand (Bridon Structures)

In the case of locked-coil strands, which are briefly presented in subsection 2.2.2 of this thesis, protection systems of various forms have been proposed. Earlier versions included varying corrosion protection in the different layers, commonly comprising galvanized outer Z-shaped wires and non-galvanized internal wires. The inside of the strand would then have a red lead filling, providing in collaboration with the final painting of the Z-shaped wires, some sort of a double barrier system for the internal wires. Under some circumstances, locked-coil strands with all wires non-galvanized have been used. Such application leaves the wires unprotected apart from the shielding provided by final painting of the outer strand surface and the interlocking effect of the Z-shaped outer wires. A notable example of the application of non-galvanized locked-coil strands is the Köhlbrand Bridge in Germany, built in 1974. The bridge cables, although assembled with red lead protection of the internal wires, experienced early deterioration due to a highly aggressive environment and poor protection techniques. Broken wires began to appear after only 3-4 years of service demanding expensive replacement of all strands (Gimsing, 1998). In modern locked-coil strands, better protection against corrosion is provided by galvanizing of both outer and inner wires in combination with the provision of a sealing compound which fills voids and prevents water infiltration. It should be noted that the main cables of the Ölfusá Suspension Bridge are composed of non-galvanized locked-coil strands installed under construction of the bridge in 1945.

4.3 Cable force estimation

This section discusses the benefits and application procedure of cable axial force assessment in cable supported bridges. Because of the structural importance of the cable system which acts as the main load bearing component of the superstructure it is often essential to determine a relatively accurate value of tension forces in the main cables and suspenders. The formulations of force determination differ in terms of boundary conditions of the considered element, indicating the applicability to stay cables, suspenders and suspender free backstays of suspension bridges where support conditions may be estimated.

4.3.1 Applications

Cases of relevant application of cable force estimation may include cable systems of aging bridges where exact values of forces are not known due to uncertainties of design values or

where renovations may have altered the force distribution as in the case of the Ölfusá Bridge. Also, progressing damage in more recently built structures may demand a thorough analysis of actual cable forces to confirm assumed design loads and assist in damage identification. This was done at the Leonard P. Zakim Bunker Hill Memorial Bridge in Boston Massachusetts (Green et al., 2009) where relatively small gaps between the stay cable bottom anchorage assembly and the steel longitudinal box girders caused concerns. By using the vibration method to estimate the stay cable tension force, assumed design loads could be verified, thus eliminating overload as the cause of the gaps. Subsequently it was concluded that unsatisfactory welding was the reason for the gaps. Further applications in terms of damage detection are described in research conducted by Siegert et al. (2007) where natural frequencies of a damaged locked-coil strand cable were measured. Six Z-shaped wires in the outer layer of the strand were cut, corresponding to a reduction of 5% of the cross section. Despite this reduction, vibration analysis of the damaged strand indicated that there was no loss of tension in the strand and the tension in the broken wires was assumed to be recovered by friction actions with the adjacent wires.

Several techniques have been used to identify installed cable force. In addition to vibration characteristics, methods based on topographic, strain or magnetoelastic property measurements are known (Caetano, 2011). The vibration method which is based on the vibrating chord theory is however the most widely used, being relatively simple in application and accurate in many cases. It relates measured natural frequencies to force through material and geometric properties according to the boundary conditions of the cable under consideration. The identification of the natural frequencies then allows for the calibration of a computational model for further analysis.

4.3.2 Theory of vibrating strings and bars

The basis for the methodology of cable force estimation where the flexural rigidity of the cable is taken into account is the partial differential equation describing the transversal motion of a uniform beam submitted to an installed axial force, T (Caetano, 2011; Siegert et al., 2007; Andersson et al., 2004).

$$EI\frac{\partial^4 y}{\partial x^4} - T\frac{\partial^2 y}{\partial x^2} + m\frac{\partial^2 y}{\partial t^2} = 0 \qquad [4.3]$$

Where E is the material modulus of elasticity, I is the moment of inertia of the beam, and m is the distributed mass per unit length. For the calculation of axial forces, the correlation between the force and natural frequency is dependent on the support conditions of the vibrating element and is described by Andersson et al. (2004): In the case of an ideal string without flexural rigidity, transversal shear deformation or sag, equation [4.3] can be omitted and the axial force becomes:

$$T = \left(\frac{2 f_i l}{i}\right)^2 m \qquad [4.4]$$

Where f_i and i are the frequency and corresponding mode number respectively and l is the span length. The vibrating string model in equation [4.4] is however only approximate, and for greater accuracy the tensioned beam model in equation [4.3] is solved to yield the axial

force of a vibrating element where flexural rigidity is taken into account but no transversal shear deformation is assumed. For pinned-pinned boundary conditions, the force is estimated as:

$$T = \left(\frac{2 f_i l}{I}\right)^2 m - EI\left(\frac{i\pi}{l}\right)^2 = \frac{m}{\kappa_{pp,i}{}^2}\left(\frac{2 f_i l}{i}\right)^2 \qquad [4.5]$$

Where κ is a factor which depends on the relation between the axial force T and the bending stiffness EI, the boundary conditions, sag, and the effect of potential shear forces. For bi-clamped boundary conditions of the element, the natural frequency for mode i may be approximated as:

$$f_i = \frac{i}{2l}\sqrt{\frac{T}{m}}\left[1 + \frac{2}{l}\sqrt{\frac{EI}{T}} + \left(4 + \frac{i^2\pi^2}{2}\right)\frac{EI}{Tl^2}\right] = k_{cc,i}\frac{i}{2l}\sqrt{\frac{T}{m}} \qquad [4.6]$$

Equation [4.6] is applicable for $i^2 < Tl^2/\pi^2 EI$. If the condition is not fulfilled, numerical solutions should be applied. Partially fixed boundary conditions yield values between the derived forces from equations [4.5] and [4.6]. In the case of a non-vertical cable such as backstays of a suspension bridge, cable sag is taken into account by reducing the modulus of elasticity with the following equation:

$$E_i = \frac{E_e}{1 + (\gamma l)^2 E_e / 12\sigma^3} \qquad [4.7]$$

Where E_e is the elastic modulus of the cable, γ is the mass density of the cable and σ is the stress in the cable.

4.3.3 Test methods and uncertainties

Similar to other vibration methods, measurements may be conducted either by ambient or forced vibration of the cables using piezoelectric accelerometers as tools of measurement. In the case of forced vibration, manual shaking and the use of an impulse hammer (Siegert et al., 2007) or pulling back the cable with ropes (Andersson et al., 2004) are amongst known methods of excitation. The choice of method varies with the required magnitude of excitation to identify the desired range of frequencies. According to Caetano (2011) it may be relevant to identify natural frequencies of 5th and higher orders for shorter cables when influence of the bending stiffness on vibration characteristics becomes significant. When the cable is not too stiff, the first natural modes will be sufficient to accurately evaluate the installed force. In many cases, ambient vibration measurements will provide the necessary excitation for the detection of needed frequencies although forced vibration will most likely be needed induce the contribution of frequencies of 100Hz or higher.

Analysis of installed cable forces in the Älvsborg Suspension Bridge conducted by Andersson et al. (2004) showed small influence of cable bending stiffness and different end restrains for long cables and suspenders. For shorter cables this effect was of considerable influence indicating the importance of proper evaluation of boundary conditions and stiffness according to the length of the cable under consideration.

4.4 Structural health monitoring

The social importance of highway bridges as well as other major civil structures demands a high level of safety and serviceability emphasizing the need to develop ways to economically operate these structures. In order to ensure structural integrity while minimizing traffic delays which tend to be expensive in terms of user costs and lost revenue to owners, structural health monitoring systems have been implemented in numerous bridge structures over the past years. Systems comprising various sensors provide the opportunity to measure relevant variables indicating the condition of the structure. It was the collapse of the Tacoma Narrows Bridge in Washington State in 1940 that forced the commencement of bridge monitoring leading to inspection and modification of some of the large suspension bridges built in USA the 1930s. Long term monitoring systems, capturing continuous readings of structural response were however developed much later. Such systems have since the 1990s been widely implemented in China, Japan, America and Europe (Xu & Xia, 2012). For illustration of the extensive usage of structural health monitoring systems Ko and Ni (2005) reported that about 40 bridges with spans of 100 m or longer worldwide had been instrumented with such systems already prior to 2006.

4.4.1 Main objectives and applications of monitoring systems

As mentioned in the introduction to this section, operational restrictions due to events such as visual inspections, maintenance or even failure are of significant cost. The implementation of structural health monitoring systems for both new and aging bridges may offer substantial benefits in terms of safety, level of service and costs. Continuous monitoring of a structure's condition will allow for an early detection of any changes indicating potential reduction in structural safety or accelerated deterioration. Critical data such as forces or displacements of relevant structural elements can be monitored and in the case of sudden changes, appropriate actions can be taken if necessary (Spuler et al., 2011). Furthermore, analysis and proper interpretation of collected data may allow for the postponement of expected remedial works or even deem them as unnecessary, saving considerable expenses.

The implementation of a long term structural health monitoring system is a process demanding various expenses in terms of installation and operational costs and may not be relevant for all bridge projects. According to (Aktan et al., 2002) health monitoring application scenarios may be classified into the following categories:

- Implementation to major bridges which typically include bridges with main spans of about 100 m or longer but also shorter span bridges classified according to their importance as lifelines or monumental value.

- Implementations to large numbers of existing short and medium span bridges. Common material properties and construction and maintenance parameters of such bridges may allow for collaboration in monitoring and maintenance strategies.

- Integrated structural and operational health and security monitoring. This implies that health monitoring can be applied to simultaneously address the

structural engineering concerns, risk, security and emergency management aspects of bridge management. This may for instance be relevant for bridges in earthquake prone areas where seismic structural response is of interest.

- Implementations to new bridges constructed of new materials or projects involving non-standardized methods. This may include the application of fiber reinforced polymer composites or high performance concretes or steels.

Some distinctions are made between the implementation of monitoring systems to new as opposed to existing bridges in terms of applicability and general benefits. Monitoring of new bridge structures provides the opportunity to measure and document forces and movements related to the construction process. Active feedback control during the erection of new structures may be necessary in terms of management of safety risks especially for complex projects involving vulnerable incomplete structural systems. By integrating monitoring into the design and construction process, assumptions and design calculations may be verified and if needed, appropriate modifications can be made in a timely manner. Knowing the structural characteristics of the as-built bridge will then allow for the calibration of a finite element model which provides a solid basis for in-service evaluations as the bridge ages and experiences variable loading conditions and potential deterioration (Aktan et al., 2002).

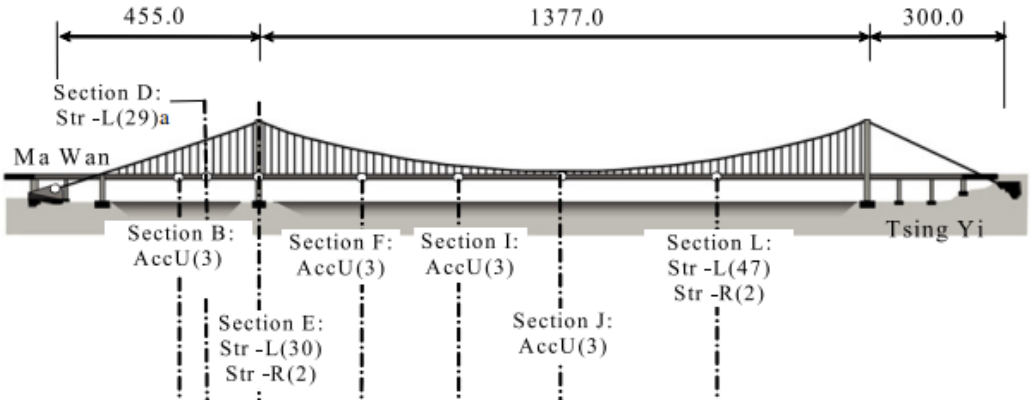

Figure 4-5: Part of the Tsing Ma Bridge sensor system (Xu et al., 2010).

Figure 4-5 gives an example of a suspension bridge where a structural health monitoring system was implemented from the beginning of construction. The figure shows the distribution of accelerometers (Acc) which measure the accelerations of the cables and bridge girder in both vertical and lateral directions, and strain gauges (Str) installed at three sections of the deck. The data is recorded with the sampling frequency of 51,2 Hz. Other measuring devices installed on the Tsing Ma Bridge but not shown in Figure 4-5 include anemometers, thermometers, displacement transducers, weigh-in-motion stations, GPS stations and level sensing stations (Xu & Xia, 2012). Different types of sensors are described in subsection 4.4.3.

In the case of existing bridges, health monitoring does enable collection of significant amounts of data even though the initial state of the structural system cannot be measured. Many of the benefits related to monitoring of new structures are therefore also valid for already existing major bridges. Premature deterioration and performance problems are

factors that make a compelling argument for implementation of health monitoring systems as well as questionable level of serviceability of bridges that have aged beyond their anticipated design periods. In many cases, monitoring over an extended period of time may be necessary and provide the most reliable assessment of causes of performance problems such as geometry changes, displacements or vibrations leading to deterioration or damage. For bridges requiring retrofit, health monitoring for a sufficient period before and after construction may reduce uncertainties regarding the actual structural conditions and how the retrofit would affect the performance of the unchanged remaining parts of the system (Aktan et al., 2002).

Figure 4-6: Ölfusá Suspension Bridge

According to the classification of health monitoring application scenarios earlier in this subsection, the relatively short span (84 m) suspension bridge at Ölfusá may well qualify for potential monitoring applications being an important road connection carrying considerable traffic amounts. Whether continuous long term monitoring is necessary is however difficult to determine before the scheduled short term monitoring vibration-based field tests have been performed and the data evaluated.

4.4.2 Design procedure for monitoring applications

Automated gathering of data and notification of any significant structural damage transmitted automatically to a remote location are ideal features of a structural health monitoring system. Development of such systems requires knowledge in various disciplines including structures, materials, damage detection, sensor technology, data collection and intelligent processing and communication (Mufti, 2001). A structural health monitoring system generally includes the following components (Xu & Xia, 2012).

- Sensory system
- Data acquisition and transmission system
- Data processing and control system
- Data management system
- Structural evaluation system

The sensory system consists of different types of sensors which are selected to identify variables such as wind, seismic and traffic loading effects, strains, displacements and accelerations and also various environmental effects. The sensors are distributed along the bridge to capture signals which are then collected and transmitted to a database through the data acquisition and transmission system. The data processing and control system controls the operation of the data acquisition system, pre-processes raw signals from the sensors and archives into a database. The system then handles post-processing and makes the collected data available for viewing. The task of the data management system is to enable further analysis of the data in the form of computational models and design files and to allow for user friendly storage and retrieval of data. Applications of the structural evaluation system vary but may include an online structural condition evaluation system and an offline structural health and safety assessment system. The former enables comparison of measured data with design values while the latter deals with loading identification, modal identification, model updating, bridge rating and damage diagnosis (Xu & Xia, 2012). Further discussion of the systemized components of structural health monitoring systems is not provided in this thesis except for a description of the sensory system given in subsection 4.4.3.

The design process of a health monitoring system generally starts with characterization of both the structure and the monitoring application. Characterization of the structure may include the review of design information and drawings, and gathering the results of past inspections and information regarding maintenance or modifications. Site visits, discussions with possible stakeholders and development of computational models of the structure are also activities involved in the process. In the case of the monitoring application; the type, level and duration of monitoring necessary to fulfill the goals of the project should be established. The second step of the process typically involves identifying which parameters need to be measured. Loading effects and the associated structural responses, serviceability criteria, environmental and security parameters and required accuracy of measurements are among the factors which determine what should be monitored. When this has been established, relevant sensors and data acquisition components are selected based on physical, electrical and thermodynamic characteristics. The number of sensors should be determined according to the size and complexity of the structure and the monitoring objectives. The final step of the process is then the development of criteria which enables meaningful and understandable presentation of monitored data (Aktan et al., 2002).

4.4.3 Sensors for structural monitoring

Wong and Ni (2009) have categorized the sensors and various monitoring equipment applicable in a sensory system into four groups for measuring the following:

1. Environmental loads and status
2. Traffic loads
3. Bridge characteristics
4. Bridge responses

The first group comprising sensors for monitoring of environmental loads and environmental status includes anemometers, temperature sensors, corrosion cells, hygrometers, barometers and rainfall gauges. The second group consisting of sensors for monitoring of traffic loads includes dynamic weigh-in-motion stations, digital video cameras and dynamic strain gauges. The third group includes portable servotype accelerometers, global positioning systems (GPS), level sensing stations and dynamic strain gauges. The fourth and last group comprising sensors for monitoring of bridge responses includes dynamic and static strain gauges, displacement transducers, global positioning systems (GPS), tiltmeters, fixed servotype accelerometers, buffer sensors, bearing sensors, and elastomagnetic sensors.

The above list of sensors is not a completely extensive list of available types although it covers most applications. The following paragraphs will introduce sensors which the author of the thesis concludes as being relevant for potential monitoring applications such as for the Ölfusá Suspension Bridge. Unless otherwise stated, information regarding the features of the different sensors is adopted from (Wong & Ni, 2009), (Xu & Xia, 2012), (Aktan et al., 2002) and (Mufti, 2001).

Accelerometers

Accelerometers are the most commonly used sensors for measurement of dynamic characteristics through forced excitation, impact and ambient vibration testing. By employing common structural damage detection methods such as those discussed in section 4.1, frequency, damping and mode shapes of a structure can be identified by post-processing collected data. Accelerometers of four main types are available: Piezoelectric type, piezoresistive type, capacitive type and servo force balance type. Piezoelectric accelerometers do not require an external power source; they are very stable and also capable of operating at a wide temperature range. The range of obtainable frequencies is fairly wide although very low frequencies (around 0,1 Hz) are generally not obtainable. According to Caetano (2011), piezoelectric accelerometers are possibly the most versatile and economic alternative in testing of cables. Piezorestrictive and capacitive accelerometers are practical for very flexible civil structures as they can measure very low frequencies. Force balance accelerometers have been applied in areas such as structural and seismic monitoring for many years.

Strain gauges

The induction of strain in civil structures is measured with foil strain gauges, vibrating wire strain gauges and fiber optic strain gauges. The least expensive and most common type is the foil strain gauge. This measurement device is about a few millimeters to centimeters in length and consists of a thin backing and a metallic foil which is fastened to the object by a suitable adhesive. The foil stretches as deformation of the object takes place and is able to measure up to a few milli-strain both under static and dynamic response. The major drawback is the sensitivity to moisture and humidity under long-term measurements which may result in problems in maintaining a stable reference point for the gauges. Another problem is that only a short distance of signal transmission between the gauge and a data acquisition unit can be obtained. The vibrating wire strain gauge determines strain by measuring the deformation induced change in vibration frequency of a thin steel wire held in tension between two end anchorages. Main benefits include easy installation on the surface or embedded in concrete and relatively long signal transmission lengths. The main disadvantages are the bulky shape of the gauges, making placement in space limited areas troublesome and that only static strain can be measured. Fiber optic sensors are small in size and immune to electromagnetic interference. They are very suitable in various situations but the high cost of both the sensors and acquisition units is a major drawback.

Displacement measurement sensors

Monitoring of displacements in bridges can provide important information on the structural condition especially in coordination with a calibrated finite element model which allows for closer analysis of the potential effects of excessive displacements. Measurement devices which are applicable to bridge displacement measurement include linear variable differential transformers, level sensing stations, global positioning system (GPS), fiber optic displacement sensors and cable extension transducers. The linear variable differential transformer is an electromechanical device which consists of a hollow metallic cylinder containing a primary and two secondary coils and movable magnetic core, commonly used for measuring relative displacements. Level sensors measure relative vertical displacement by measuring variation of the water level in filled cells. The accuracy of these two methods is about and under 0,5 mm. Regular GPS measurements, using signals from four or more satellites only yield accuracy of the order of a meter which is insufficient for displacement monitoring of bridges which should be in the order of a centimeter. However a nominal accuracy of about a centimeter may be obtained by incorporating a base reference station and a number of mobile units. An advantage of GPS is that it does not require a physical reference point on the bridge to measure absolute displacements. Fiber optic displacement sensors have been used for bridge testing and monitoring applications, especially in Europe and cable extension transducers are commonly used to measure position and linear displacements by the use of a steel cable wound on to a spool.

Anemometers

Wind measuring devices, although most relevant for long span suspension bridges where wind induced buffeting and torsional stability may be of concern, yield beneficial information regarding the wind loading environment where needed.

Thermometers

Temperature changes are known to have a significant influence on deflections and deformations in bridges. Both ambient air temperature and the temperature of structural elements are commonly measured and reveal information regarding factors such as thermal stresses which can damage bridges, and also in connection with deflection measurements.

Acoustic emission sensors

Acoustic emission monitoring systems typically employ an array of high frequency sensors operated continuously to detect the resulting energy release of an occurring wire failure. According to Nair and Cai (2010) the waves of released energy are converted into electrical signals using sensors of piezoelectric elements which are chosen according to sensitivity required for the investigation.

4.5 Monitoring of loading effects

The main objectives of structural health monitoring of bridges include monitoring of the loading conditions to enable early detection of possible damage or deterioration and ensure structural and operational safety (Ko & Ni, 2005). The close monitoring of loading conditions is especially important in the case of suspension bridges which are often located in unique environments and may experience harsh loading conditions. Dead load, traffic load, temperature load, wind load, and seismic load are generally the main design loads for suspension bridges. While the dead load of the structure can be determined quite accurately from design documents, other loads are most often adopted from design standards or measured from scaled models making in-service structural responses hard to predict. A well designed monitoring system will assist in analyzing the actual responses of the structure and provide valuable data for future designs (Xu & Xia, 2012). This section will briefly address structural monitoring of the types of imposed loads which may be considered to be the most relevant with regard to the condition and operational safety of the Ölfusá Suspension Bridge.

4.5.1 Traffic loading effects

Random loading of non-stationary vehicles imposes complex loading conditions on suspension bridges carrying traffic loading. Axle loads, axle configuration, vehicle weight and speed, number of vehicles on the bridge and bridge configuration are parameters that affect the load distribution in the bridge. Monitoring of the traffic on the bridge is then beneficial as actual and design loads may be compared to ensure the safety and functionality of the bridge (Xu & Xia, 2012; Mufti, 2001).

The implementation of a traffic monitoring system begins with the selection of appropriate sensors and corresponding data acquisition units and design of the system layout. Common devices used for traffic monitoring include dynamic weigh-in-motion stations for recording of highway traffic conditions, displacement transducers, accelerometers, and strain gauges. The latter three devices were described in subsection 4.4.3. The benefits of keeping highway traffic records include possible extraction of different statistical data that once pre-processed can be analyzed to yield valuable data regarding highway traffic condition

and load distribution. By using these data, axle load distribution and gross vehicle weight distribution may be identified and applied in the formation of an axle load spectrum or a gross vehicle weight spectrum. These spectra may be used for fatigue life estimation of the bridge which is conducted by simulating the equivalent number of passages of a standard fatigue vehicle, derived using the spectra as basis (Xu & Xia, 2012).

4.5.2 Corrosion effects

Corrosion in bridge structures is generally associated with corroding reinforcement bars or tendons embedded in concrete mixture or corroding suspended or stayed cables. Counteracting methods such as quality control requirements relating to concrete mixtures and the application of various surface coatings are often provided in the construction period. Structures located in a coastal environment are especially vulnerable to corrosion. The ingression of chloride ions and carbon dioxide to reinforcement bars and tendons in concrete structures induces deterioration in the form of corrosion resulting in potential crack formation and spalling of the concrete cover. Techniques that have been applied in evaluation and monitoring of steel corrosion in reinforced concrete include visual inspection, nondestructive testing, and electrochemical methods. Only significant corrosion can be detected by visual inspection and electrochemical techniques are destructive methods where concrete cores are required for laboratory testing. Some non-destructive test methods such as ultrasonic pulse velocity- and radiography methods are discussed in subsection 4.1.6. Sensors which are able to monitor corrosion affecting factors such as chloride content in concrete structures have also been developed (Xu & Xia, 2012). In the case of external cables of suspension and cable stayed bridges, monitoring of corrosion effects is carried out in the form of visual inspections, or methods including for example magnetostrictive and acoustic emission techniques such as described in section 4.1.

Increased cross sectional area of cables may be considered as a sign of potential internal corrosion because rust is 4-8 times larger in volume than steel. This indicator especially applies for cables of open section. Corroding suspenders may possibly be identified by cracks between threads, rust colored drops of water and increased diameter. In the case of broken threads due to construction or material defects, or traffic overload, the cable becomes more susceptible to corrosion and the bearing capacity is reduced accordingly. Reparative measures may include surface treatment, sealing of the affected area or replacing of the damaged cable (Statens Vegvesen, 2000). Figure 4-7 (Guðmundsson, 2011b) shows a broken thread in the western main cable of the Ölfusá Bridge. In the cited report it is mentioned that the locked coil strands have in several places become sparse, making the unprotected internal wires susceptible to the intrusion of water and humidity. Furthermore, an example presented by Statens Vegvesen (2000) is worth mentioning where three broken threads due to traffic overload were identified through visual monitoring in a cable of similar type. The recommended measure in that case was to seal the affected area within three years.

Figure 4-7: Broken thread in the Ölfusá Bridge main cable

4.5.3 Other effects

Seismic effects are of course of concern due to the level of seismological activity in the vicinity of the Ölfusá Bridge. The objective of this part of the thesis has however been to focus more on structural health monitoring aspects relevant to operation of the bridge under self-weight, traffic loading and constant environmental loading conditions and less on accidental loading and natural hazards. Further relation to seismic effects is therefore omitted. Temperature and wind induced effects have neither been discussed in detail whereas these types of loads have greater influence on longer span suspension bridges and are not suspected to become deciding factors for the structural life of the Ölfusá Bridge.

4.6 Summary of damage detection and structural health monitoring

The objective of this chapter of the thesis has been to provide an overview of damage detection- and structural health monitoring techniques applicable for suspension bridges by summarizing reported methods in a suitable level of detail. In section 4.1, structural damage detection methods where divided into vibration methods and nondestructive methods. Two methods of each category, selected with regard to applicability to small scale suspension bridges such as the Ölfusá Bridge, were described while less relevant techniques were briefly outlined. Frequency change- and mode shape analysis where selected as vibration-based methods, both of which are directly related to the modal analysis conducted in chapter 3 of this thesis and may be concluded as effective in terms of model calibration and damage detection at a global structural level. The natural frequency, being the most fundamental vibration parameter, is preferable for research of variably scaled structures and the scheduled vibration tests and further research of the Ölfusá Bridge will involve frequency-based analysis. The nondestructive methods that were described in the chapter were the magnetostrictive technology and the acoustic emission method. These two methods may provide damage recognition at a more detailed local level of the structure and may possibly be considered in potential future application at the Ölfusá Bridge. Such steps will although depend on a more thorough evaluation of potential cable damage location whereas detection with the magnetostrictive technology is problematic at anchors and cable clamps. Also the acoustic emission method is more widely used in bridges comprising a parallel cable system, leaving some uncertainty towards the applicability to the Ölfusá Bridge which comprises locked coil strands as main cables.

Section 4.2 discusses the effects of cable corrosion and gives a brief overview of practical cable protective systems and section 4.3 outlines the procedure of cable force evaluation. The tension force in suspenders and stayed cables such as non-suspended backstays in suspension bridges may be estimated by measuring the natural frequency of the cable under ambient or forced disturbance. The theory which links the measured frequency to an estimated axial force depends on the support conditions of the cable and is briefly explained in the section.

An overview of structural health monitoring is given in sections 4.4 and 4.5. In the text of this 4th chapter of the thesis, it is attempted to differentiate between structural damage detection and structural health monitoring in the sense that the prior may refer to certain

measures taken to identify suspected damage while the latter refers to a more constant surveillance over a longer time period. The main objectives of health monitoring have been described as early detection of potential defects or deterioration which may be of concern to the structural integrity, enabling necessary precautions to be taken in time. A compelling argument for continuous monitoring may also be noted as maintenance and rehabilitation actions can be scheduled with accurate state of the structure in mind and potentially even omitted. Furthermore, a commonly applied design methodology for monitoring systems is explained and different types of measurement devices are described. The Ölfusá Bridge, being an important road connection may well qualify for some degree of constant monitoring. Further research, following the planned vibration tests will however help determine whether such steps become necessary.

5 Concluding remarks

This thesis has presented an introductory discussion on suspension bridges, a structural health oriented finite element model of the Ölfusá Suspension Bridge, and a literature overview of reported structural damage detection- and health monitoring methods.

The main focus of the thesis has firstly been the modeling process, involving two versions of the Ölfusá Bridge model; one representing the original configuration of the bridge from 1945 and another one of the present configuration which includes a concrete deck of considerably heavier construction, installed in 1992. Secondly, structural damage detection- and health monitoring methods where described to some level of detail with the current condition of the Ölfusá Bridge and applicability for structural integrity evaluation of a small scale suspension bridge in mind.

The main objective of creating a finite element model representing the original state of the bridge was to obtain some level of model validation by comparing analytical results with original design documents and four load tests conducted in 1946. The most concurrent findings of this process were that the difference in main cable tensile forces at the middle of the main span was around 9%, and comparison of the two most reliable load tests showed a difference of around and less than 20%. These results were concluded to indicate the ability of the structural model to adequately describe the actual behavior of the original structure at a global level. Furthermore, a modal analysis was conducted and compared with calculations published in 1982. Some resemblance was noted from those results but due to the different nature of the calculation procedures used and assumptions made, the comparison was mainly performed with educational purposes in mind rather than further validation of the model.

The model representing the present structural configuration of the bridge with the heavier deck plate was analyzed to yield results describing the static and modal behavior, and also traffic induced responses of the structure. The static analysis showed a 49% increase in self-weight of the main span of the current structure compared to the original one. The expected uneven force distribution between cable planes was confirmed whereas the upstream side of the deck which is heavier than the downstream side due to the unsymmetrical construction, experienced 11 mm larger deflections than the downstream part, and around 5% higher main cable and suspender forces, respectively. Computed deflections at the middle of the 84 m long span resulting from self-weight went from a documented value of +147 mm (hogging) for the original structure to a nearly horizontal +8 mm in the upstream part of the current deck. The computed middle span cable and suspender forces suffered an increase of 37% and 40%, respectively and the absolute maximum main cable force occurring at the west tower was subjected to an increase from 3057 kN to 4188 kN which is a 37% addition to the maximum tensile forces before the construction of the newer bridge deck. For the six strands of 2176mm^2 cross sectional area, comprising each main cable, that means a stress increase from 234-321 MPa. The modal analysis that was carried out for this model was discussed with regard to preferable positioning of accelerometers to capture the movements of the significant modes, leading to an example of a potential vibration test set-up presented in the summary of the 3rd

chapter. The traffic analysis part consisted of the analysis of trucks weighing in the range of 200–1000 kN driving over the bridge and an estimation of the main cable factor of safety. A characteristic load combination implementing load model 1 according to Eurocode 1, gave a maximum un-factored cable force of 6453 kN (494 MPa) yielding the factor of safety of 2,4 when compared with the full initial bearing capacity of 15900 kN (1218 MPa). This is a low value compared with the initial factor of 4 and an actual value is likely to be even lower because potential deterioration of the cables is not accounted for.

From the 4th chapter of this thesis, presenting structural damage detection- and health monitoring applications, it can be concluded that vibration testing, followed by model calibration is probably the most practical next step in the evaluation of the Ölfusá Bridge. The implementation of methods involving magnetostrictive- and acoustic emission techniques for a more detailed identification of potential structural anomalies is not considered as imminent at the moment. Also, it is difficult to determine whether long term health monitoring of the bridge is necessary before model calibration and complete analysis after the vibration tests have been conducted.

Further evaluation of the cable condition is concluded to be the most important topic of near future research for the Ölfusá Bridge. This thesis has provided an estimation of the force distribution between cable planes but the actual bearing capacity remains at an uncertain level. The temporary removal of single cable clamps has been suggested to enable inspection of the most vulnerable part of the main cable. This would possibly give a more decisive idea of the rate of cable degradation and provide a more accurate value of effective cable cross section. The effects of degrading cable cross section on middle span deflections were illustrated in the 3rd chapter, also implying a practical usability of monitoring the level of the bridge deck by measurements at regular time intervals or by continuous remote monitoring. Regular measuring of the natural frequencies in the backstays, providing an estimation of installed cable force is also considered to be beneficial.

Interesting research topics that were omitted from this thesis due to time extent limitations are the construction of a finite element model comprising the whole bridge structure including the side span decks, and also the definition of a staged construction analysis case. Such type of analysis would involve nonlinear material characteristics and be used to simulate the effects of unloading the structure when removing the original bridge deck and reloading when installing the current one. If the measures discussed in this section lead to the necessity of more decisive actions, a lighter bridge deck construction, design of a structural monitoring system, traffic regulations and a sooner construction of a new bridge are considerations worth mentioning.

References

Åkesson, B. (2008). *Understanding bridge collapses.* Leiden, The Netherlands: Taylor & Francis/Balkema.

Aktan, A., Catbas, F., Grimmelsman, K., & Pervizpour, M. (2002). *Development of a model health monitoring guide for major bridges. Federal report no. DTFH61-01-P-00347.* Philadelphia: Drexel Intelligent Infrastructure and Transportation Safety Institute.

Allemang, R., & Brown, D. (1983). Correlation coefficient for modal vector analysis. *1st International modal analysis conference,* (pages 110-116). Kissimmee.

Andersson, A., Sundquist, H., & Karoumi, R. (2004). Evaluating cable forces in cable supported bridges using the ambient vibration method. *The 4th International cable supported bridge Operator´s Conference, June 16-19th.* Copenhagen, Denmark.

Arcelor. (2006). Sections: Beams, channels and merchant bars.

Barker, K. J., & Tozser, O. (2011). The use of acoustic monitoring to extend the life of Bowdon View Bridge. *35th Annual Symposium of IABSE / 52nd Annual Symposium of IASS / 6th International Conference on Space Structures.* London: Taller, Longer, Lighter - Meeting growing demand with limited resources: IABSE-IASS 2011 London Symposium Report.

Bates, W. (1991). *Historical Structural Steelwork Handbook.* London: The British Constructional Steelwork Association Limited.

Caetano, E. (2011). On the Identification of Cable Force from Vibration Measurements. *IABSE-IASS-2011.*

Cawley, P., & Adams, R. (1979). The locations of defects in structures from measurements of natural frequencies. *Journal of strain analysis,* 49-57.

CEN: European Comittee for Standardization. (2005). *Eurocode 3: EN 1993-1-11, 2005 - Design of steel structures Part 1.11: Design of structures with tension components.* Brussels: European Comittee for Standardization.

CEN: European Committee for Standardization. (2003a). *Eurocode 1: EN 1991-1:2002. Actions on structures - Part 1-1: General actions — Densities,.* Brussels: European Committee for Standardization.

CEN: European Committee for Standardization. (2003b). *Eurocode 1: EN 1991-1:2002. Actions on structures - Part 2: Traffic loads on bridges.* Brussels: European Committee for Standardization.

CEN: European Committee for Standardization. (2003c). Eurocode 8: EN 1998-1:2003. Design of structures for earthquake resistance - Part 1: General rules, seismic actions and rules for buildings. Brussels: European Committee for Standardization.

Chopra, A. (2007). *Dynamics of structures - Theory and applications of earthquake engineering.* Upper Saddle River: Pearson Prentice Hall.

Computers and Structures, (2011). *Sap2000 - Integrated Structural Analysis & Design Software.* Berkeley, California: Computers and Structures Inc.

Cook, R. (1995). *Finite element modeling for stress analysis.* Toronto: John Wiley & Sons, Inc.

Cook, R., Malkus, D., Plesha, M., & Witt, R. (2002). *Concepts and applications of finite element analysis.* John Wiley & sons. Inc.

Doebling, S., Farrar, C., & Prime, M. (1998). A summary review of vibration-based damage identification methods. *The shock and vibration digest*, 91-105.

Dorman Long & Co. LTD. (14. June 1945). Ölfusá Bridge, Iceland. Stress sheet - DRG No. G. 786.

ESDEP - *Lecture 15B.9: Suspension Bridges*. Retreived in January 2012 from web source: http://www.fgg.uni-lj.si/kmk/esdep/master/wg15b/l0900.htm#SEC_1

Gimsing, N. J. (1998). *Cable supported bridges - concept and design, 2nd edition.* Chichester: John Wiley & Sons Ltd.

Green, T., Moore, M., & Hannen, R. (2009). Stay Cable Vibration Testing at the Leonard P. Zakim Bunker Hill Memorial Bridge . *Don't Mess with Structural Engineers: Expanding Our Role, Proceedings of the 2009 Structures Congress.* American Society of Civil Engineers.

Guðmundsson, G. V. (2011a). *Ástand kapla í hengibrúm.* Reykjavík: EFLA.

Guðmundsson, G. V. (2011b). *Brú á Ölfusá - Mat á ástandi kapla.* Reykjavík: EFLA.

Icelandic Road Administration. (January 2011). *Brúaskrá*. Retreived in April 2012 from: http://www.vegagerdin.is/Vefur2.nsf/Files/Bruaskra-a-thjodv/$file/Bruaskra-a-tjodvegum.pdf

Icelandic Road Administration. Archived drawings of Ölfusá Suspension Bridge.

Ko, J., & Ni, Y. (2005). Technology developments in structural health monitoring of large-scale bridges. *Engineering Structures*, 1715-1725.

Kwun, H., & Bartels, K. (1998). Magnetostrictive sensor technology and its applications. *Ultrasonics*, 171-178.

Kwun, H., Kim, S., & Light, G. (April, 2011). Magnetostrictive sensor technology for long-range guided wave inspection and monitoring of pipe. *NDT Technician*, 6-8.

Malhotra, V., & Carino, N. (2004). *Handbook on nondestructive testing of concrete, second edition.* West Conshohocken: ASTM International.

Mayrbaurl, R., & Camo, S. (2004). *NCHRP Report 534 - Guidelines for inspection and strength evaluation of suspension bridge parallel wire cables.* Washington DC: Transportation research board.

Mufti, A. (2001). *Guidelines for structural health monitoring.* Winnipeg, Canada: Intelligent Sensing for Innovative Structures.

Nair, A., & Cai, C. (2010). Acoustic emission monitoring of bridges: Review and case studies. *Engineering structures*, 1704-1714.

Nakamura, S., & Suzumura, K. (2011). *Corrosion of bridge cables and the protection methods.* IABSE-IASS conference 2011.

NYPL Digital Library. (March 2011). *Mid-Manhattan Picture Collection / New York City - - bridges*. Retreived in January 2012 from web source: http://digitalgallery.nypl.org/nypldigital/dgkeysearchresult.cfm?keyword=Brooklyn+Bridge

Pálsson, Á. (1947). Prófun Ölfusárbrúar14.12.1946 – handreikningar formbreytinga. Icelandic Road Administration.

Pure Technologies. (without date). *Pure Technologies.* Retreived in April 2012 from: http://www.puretechltd.com/services/cable_scan.shtml

Rankin, S., Gagnon, C., & Sluszka, P. (2006). *Inspection, Evaluation and Monitoring of Suspension Bridge Cables.* New York: ASCE.

Ren, W.-X., Blandford, G., & Harik, I. (2004). Roebling suspension bridge. I: Finite-element model and free vibration response. *Journal of Bridge Engineering*.

Rytter, A. (1993). *Vibration based inspection of civil engineering structures, Ph.D. dissertation.* Alborg: Aalborg University.

Salawu, O. (1997). Detection of structural damage through changes in frequency: A review. *Engineering structures*, 718-723.

Siegert, D., Dieng, L., Goursat, M., & Toutlemonde, F. (2007). Frequency Monitoring of Stay-cables. *2007 IMAC-XXV Conference.*

Sigbjörnsson, R., & Bessason, B. (1982). *Jarðskjálftasvörun Hengibrúa - Jarðskjálftaálag á brýr á Suðurlandi, Áfangaskýrsla nr. 3.* Reykjavík: Verkfræðistofnun Háskóla Íslands.

Song, H., & Dong, W. X. (2010). *Zhoushan Xihoumen Bridge - The world´s longest box-girder suspension bridge.*

Spuler, T., Gianni, M., Berger, R., & O´suilleabhain, C. (2011). Modern remote structural health monitoring - providing long-term confidence in a structure´s condition. *35th Annual Symposium of IABSE / 52nd Annual Symposium of IASS / 6th International Conference on Space Structures, London, September 2011*. London: Taller, Longer, Lighter - Meeting growing demand with limited resources: IABSE-IASS 2011 London Symposium Report.

Statens Vegvesen. (2000). *Håndbok 136 - Inspeksjonshåndbok for bruer – Veiledning.* Oslo.

Williams, C., & Salawu, O. (1995). Bridge assessment using forced-vibration testing. *Journal of structural engineering*, 161-173.

Wilson, E. (2002). *Three-Dimensional Static and Dynamic Analysis of Structures, 3rd edition.* Berkeley: Computers and Structures, Inc.

Wong, K.-Y., & Ni, Y.-Q. (2009). *Chapter 123 - Modular architecture of SHM system for cable-supported bridges. In Encyclopedia of structural health monitoring edited by Boller, C., Chang, F.K., and Fujino, Y.* Chichester: John Wiley & Sons.

Xu, Y., Li, Q., Wu, D., & Chen, Z. (2010). Stress and acceleration analysis of coupled vehicle and long-span bridge systems using the mode superposition method. *Engineering Structures*, 1356-1368.

Xu, Y.-L., & Xia, Y. (2012). *Structural health monitoring of long span suspension bridges.* New York: Spon Press.